

# Influence of the anisotropy of sisal fibers on the mechanical properties of high performance unidirectional biocomposite lamina and micromechanical models

Bernardo Zuccarello\*, Carmelo Militello, Francesco Bongiorno

*University of Palermo - Department of Engineering, Viale delle Scienze, 90128 – Palermo, Italy.*

\* Corresponding author email: [bernardo.zuccarello@unipa.it](mailto:bernardo.zuccarello@unipa.it)

## ABSTRACT

High performance biocomposites reinforced by sisal fibers, are between the most promising materials that could be used in various fields, from automotive to civil constructions, thanks to their good mechanical performance, as well as to the low cost and the great availability of the fiber. Nevertheless, at present their practical use is prevented by the limited knowledge of their mechanical performance. The results of this analysis have shown that the intimate fibrillar structure of the sisal fiber is associated with a high anisotropy involving not only the elastic parameters, but also the damage processes with a typical fiber splitting phenomena, that influence noticeably the biocomposite strength under transversal tensile, longitudinal compression and shear loading. Also, they have permitted to implement accurate micromechanical models that can be used at the design stage, in all those structural applications where low cost green biocomposites reinforced by sisal long fiber could be advantageously used.

**Keywords:** A. Biocomposite; A. Natural fibers; B. Anisotropy; C. Micro-mechanics

## 1. INTRODUCTION

Composite materials reinforced by natural fibers are increasingly used in various fields of the civil and industrial sectors [1-15], especially for non-structural applications (filling material, soundproofing, dashboard etc.). Between the various natural fibers used to the development of such interesting materials [16-25], the sisal fiber is very attractive because of its good mechanical properties associated to many other advantages as high availability in the current market, low cost, low embodied energy, low skin irritability, low damageability and good toughness [26-37]. The sisal fiber is extracted by a plant called agave sisalana, cultivated extensively in Africa and South America and constituted by a few dozen flat and elongated leaves (Fig.1a), each containing a thousand structural fibers (Fig.1b) concentrated along the leaf perimeter. Due to the low cost and the low weight of the sisal fiber, the relative biocomposites are typically characterized by cost and weight lower than any composite reinforced by synthetical fibers; also, unlike synthetical composites, cost and weight decrease if the fiber volume fraction increases.

Also, recent studies on epoxy and PLA (Polylactic Acid) matrix biocomposites reinforced with sisal fibers [38-44] have allowed the development of an unidirectional lamina characterized by high mechanical performances (tensile strength up to about 500 MPa and stiffness up to about 30 GPa), which can be used advantageously for the implementation of ecofriendly or renewable laminates for the replacement of technical metals (steel, aluminum etc.) and common GFRP (Glass Fiber Reinforced Polymer) in structural and semi-structural applications. Thanks to the very low specific mean weight (about 13.5 kN/m<sup>3</sup>), lower than any synthetic fiber reinforced composite, such a lamina exhibits a specific longitudinal tensile strength that is higher than common steels and good aluminum alloys, and comparable with that of GFRPs used for structural applications [42-43]. Also the specific longitudinal stiffness is only slightly less than steel and aluminum ones, and higher than that of unidirectional GFRPs.

Unfortunately, the most research works reported in literature focused only the performance of biocomposites under simple tensile/bending loading [26-38], or the possible treatments [45-52] able to improve the mechanical properties of the sisal fiber and the fiber-matrix adhesion. Consequently, as it occurs also for most biocomposites proposed in literature [16-25], the practical use of the sisal reinforced laminates (cross-ply, angle-ply etc.) still requires further studies for a complete knowledge of the mechanical behavior of the fiber as well as of the biocomposite unidirectional lamina under the various loading conditions that can occur during the actual service. In more detail, the lack of knowledge encompass the mechanical anisotropy of the sisal fiber and its influence on the properties of the corresponding biocomposites, as well as the consequent availability of micro-mechanical models that can be used both for the estimation of the transversal and shear properties of the fiber, and for a reliable prediction of the mechanical behavior of a generic unidirectional lamina under various loading conditions.

In more detail, regarding the anisotropy of the fiber, the direct analysis of the intimate structure of the sisal fiber (see Fig.1c and d), that is constituted by a multitude of hollow quasi-cylindrical sub-fibers aligned with the fiber axis, suggests a high mechanical anisotropy which to date, unfortunately, has not been properly considered in the analysis of the corresponding biocomposites, that has been always performed approximately by assuming an isotropic behavior.

Most probably, also the low mechanical strength of randomly short natural fiber biocomposites widely observed in literature [2, 27-32] is related to the fiber anisotropy, although to date the most researchers have attributed this only to the supposed low strength of the fiber-matrix interface, due to the hydrophilic nature of the natural fibers. This has led to relevant research works focused on possible fiber treatments [45-52] in order to improve the fiber-matrix adhesion.

The exam of the literature shows that very few work have been addressed to the anisotropy of the natural fibers [53-58] and they have been mainly addressed to the jute fiber [53, 54] or to the development of theoretical model involving the cellulose content and the spiral angle dependency [55].

In more detail, in [53] Cichocki et al. have analyzed the anisotropy of the jute fiber by using the experimental results of the corresponding biocomposites, and proper micromechanical models.

In [54] instead, Thomason has studied the possible correlation between the low strength of a random short jute fiber reinforced polypropylene and the anisotropic internal fiber structure. His results emphasize the importance of the knowledge of the fiber anisotropy for the correct prediction of the mechanical properties of the relative biocomposites, although the fiber strength anisotropy has not been examined.

Only in [56, 57] the authors consider the anisotropy of the sisal fiber but their study is quite approximate and not complete; in fact, they consider only the main elastic moduli, neglect the influence of the fiber volume fraction, and estimate the fiber shear modulus without proper shear tests on composites. Also, such works do not consider any compressive loading case and, above all, none estimation of the strength anisotropy of the fiber is performed; consequently their results are not useful for the prediction of the actual influence of the fiber anisotropy on the mechanical performance of a generic sisal reinforced biocomposite used in practical applications.

Regarding the implementation of micromechanical models that can be used for the reliable description of the biocomposites performance by varying the fiber volume fraction, the examination of the literature shows that no study has been addressed properly to this important scope, and also the above mentioned works [53-58] have considered only the elastic properties by using always (also for the shear properties) the simple inverse rule of mixture, i.e. the approximated Voight model and the Reuss model for longitudinal and transverse properties respectively.

In order to give a contribution to the accurate knowledge of the anisotropic behavior of the sisal fiber, by considering both the elastic moduli and the mechanical strength, in this study a systematic experimental tests campaign has been performed by considering all the possible loading conditions that can occur on an unidirectional lamina, by varying the fiber volume fraction in the common range used for structural applications. The accurate examination of the results of such experimental campaign has allowed the accurate evaluation of the main anisotropic parameters that govern the mechanical behavior of the fiber and its influence on the relative unidirectional lamina; also, the best fitting of the experimental results has permitted to select (or implement properly) the optimal micromechanical models that are able to take into account the sisal fiber anisotropy; consequently, they can be advantageously used at the

design stage for the reliable prediction of the mechanical properties of the corresponding high-performance biocomposites.

## 2. MATERIALS AND METHODS

### 2.1. Matrix

The green epoxy resin used for the manufacturing of the biocomposites is called SUPERSAP CNR, and is provided by Entropy Resin Inc. (CA), USA [59]. As widely shown in [39-42], this matrix exhibits a quite linear elastic behavior with a tensile Young's modulus  $E_m \approx 2.5$  GPa, a Poisson's ratio  $\nu_m \approx 0.38$  and a brittle failure which corresponds a tensile strength  $\sigma_{m,R} \approx 45$  MPa and a failure strain  $\varepsilon_{m,R} \approx 2.5$ . These mechanical characteristics have been indicated by the provider and confirmed by proper tensile test carried out before the biocomposite manufacturing. Also, proper shear tests have permitted to detected a shear strength  $\tau_{m,R} \approx 25$  MPa.

### 2.2. Fibers

As mentioned above, the reinforcement of the high performance biocomposites considered in this work, has been obtained by using high quality long sisal fibers, obtained by South American plantations (Fig.1a) and provided by the Mellau-Teppich GmbH & Co (Austria). In order to maintain a high degree of renewability of the biocomposites, no additional surface treatment have been carried out.

Taking into account the potential high scattering of the mechanical properties of natural fibers [39-42], the longitudinal tensile properties of the fiber batch used in the present work (Fig.1b) has been accurately determined by preliminary single fiber tensile tests carried out according the ASTM D3822 / D3822M standard [60], by using an INSTRON 3367 universal testing machine equipped by an optical extensometer, and the approach exposed in [42] to measure the trasversal fiber section.

### 2.3. Manufacturing of the high-performance unidirectional laminae

In accordance with previous works of the same authors [39-44], the high performance biocomposite unidirectional laminae considered in the present work, have been obtained by using unidirectional "stitched" type fabrics (having a mean weight of about 210 g/m<sup>2</sup>) preliminary made in laboratory by a particular procedure consisting in the manual alignment/stretching of the fibers (Fig.2a) followed by the execution of transverse seams at regular intervals of about 50 mm (Fig.2b).

In order to cover the typical range of the fiber volume fraction  $V_f$  used for structural applications [61, 62], i.e.  $0.2 \leq V_f \leq 0.7$ , such unidirectional fabrics have been used for the manufacturing of single-layer laminates type  $[0_x]$ , with  $x = 4, 6, 8, 10, 12$  and  $14$  for  $V_f$  values equal to 0.2, 0.3, 0.4, 0.5, 0.6 and 0.7. For all the fiber volume fractions considered, in order to obtain the desired thickness of 3 mm, calibrated shims have been located inside the mould before pressing the panel.

In detail, in order to obtain high quality laminates (with limited voids and without direct contact between the fibers), after the preliminary hand lay-up performed inside a rectangular mold (see Fig.3a) having dimension of 340 x 190 mm, a successive optimal compression moulding process [41, 42], has been applied by using a 100-tons hydraulic press (Fig.3b). In detail, a thermomechanical curing process having a total duration of 5 hours (3 hour at a constant temperature of 80° C and 1 hour for the increasing and decreasing phases) with curing pressure included in between 0.06 MPa ( $V_f=0.2$ ) to 6 MPa ( $V_f=0.7$ ) and gelling time in the range from 0.25 hours ( $V_f=0.2$ ) to 0.5 hours, has been used (see reference [42] for more details). From such panels (see Fig.3c), proper specimens have been extracted for the subsequent experimental tests described in detail in the following.

#### 2.4. Mechanical testing under various loading conditions

As mentioned above, the accurate analysis of the anisotropic behavior of the sisal fiber, in terms of elastic properties and mechanical strength, has been performed through a complete experimental testing of the reinforced unidirectional lamina carried out by considering the five main loading conditions [61, 62]: longitudinal tensile loading, transversal tensile loading, shear loading, longitudinal compressive loading and transversal compressive loading. In more detail, the longitudinal and the transversal tensile tests has been carried out by using an INSTRON 3367 testing machine (see Fig.4) and specimens instrumented by a longitudinal extensometer type HBM (base length  $b=25$  mm) and a transversal VISHAY electrical resistance strain gauge (base length  $b=8$  mm); in accordance with the ASTM D3039 / D3039M [63] standard, specimens having dimension of 15x250x3 mm and 25x175x3 mm have been used for longitudinal and transverse test respectively.

The longitudinal and transverse compressive tests has been performed instead in accordance with the ASTM D 6641/D 6641M standard [64]; in detail, in this cases the compressive strains were monitored by means of a VISHAY electrical resistance strain gauge (having  $b = 12$  mm).

The particular devices used for the shear tests accomplished in accordance with different approaches, are described in detail in section 3.3.

### 3. RESULTS AND DISCUSSION

The preliminary “single fiber” tensile tests carried out on the fiber batch used in this work, have provided the following mean values and standard deviations of the main mechanical parameters: longitudinal tensile strength  $\sigma_{L,R}^{(f)} = 675$  MPa (standard deviation of about  $\pm 11\%$ ), longitudinal tensile Young’s modulus  $E_L^{(f)} = 40,10$  GPa (standard deviation of about  $\pm 14\%$ ) and ultimate longitudinal tensile strain  $\varepsilon_{L,R}^{(f)} = 1.73\%$  (standard deviation of about  $\pm 15\%$ ).

### 3.1. Mechanical behavior under longitudinal tensile loading

The results obtained by longitudinal tensile tests confirm, as just obtained in [41] on similar fibers, that the longitudinal tensile strength  $\sigma_{L,R}$  and the longitudinal Young's modulus  $E_L$  obey the rule of mixtures (ROM), with deviations in general always lower than 10% (see Figs.5a and 5b). In detail, Fig.5a shows how  $\sigma_{L,R}$  varies with  $V_f$  in accordance with the following ROM [61, 62]:

$$\sigma_{L,R} = 0.85\sigma_{L,R}^{(f)}V_f + \sigma_m^*(1 - V_f) \quad (1)$$

in which  $\sigma_m^*$ , is the matrix stress that occurs at the fiber failure strain  $\varepsilon_{L,R}^{(f)}$  equal to 0.0173, whereas  $\sigma_{L,R}^{(f)}$  is the fiber tensile strength determined by the previous single fiber tensile tests (see section 2.2). The constant 0.85 that appears in Eq.(1), is provided by the best fitting procedure of the experimental data and corresponds to the well-known corrective coefficient commonly applied to the fiber tensile strength [61, 62] in order to take into account the main influence parameters (fiber damaging during biocomposite manufacturing, fiber misalignment etc.); its relatively high value confirms the good quality of the biocomposites as well as the low damageability of the sisal fiber. No macroscopical debonding (no trasversal swelling of the failure specimen is observed) or pull-out phenomena (no long fiber segment is observed) have been observed in the longitudinal tensile tests, confirming the good matrix-fiber adhesion.

Fig.5b shows instead the good agreement of the longitudinal tensile Young's modulus  $E_L$  detected experimentally by varying the fiber volume fraction  $V_f$ , with the well-known ROM [61, 62]:

$$E_L = E_L^{(f)}V_f + E_m(1 - V_f) \quad (2)$$

written by using the values  $E_L^{(f)} = 40.1$  GPa (see section 2.2) and  $E_m=2.5$  GPa; also in this case the deviation observed are less than about 10%.

Finally, Fig.5c shows the experimental results obtained in terms of major Poisson's ratio  $v_{LT}$  by varying  $V_f$ . The comparison of the straight line fitting the experimental values (passing also to the y-intercept point corresponding to the matrix Poisson's ratio  $v_m = 0.38$ ) and having the following expression:

$$v_{LT} = 0.61 V_f + 0.38 (1 - V_f) \quad (3a)$$

with the well-known ROM provided by the micromechanics for the major Poisson's ratio  $v_{LT}$  of an unidirectional lamina [61, 62], i.e:

$$v_{LT} = v_{LT}^{(f)}V_f + v_m(1 - V_f) \quad (3b)$$

permits immediately to recognize as the major Poisson's ratio  $v_{LT}^{(f)}$  of the sisal fiber takes the value 0.61, superior to the isotropic limit of 0.5. Such a value corroborates the expected anisotropic elastic behavior of the sisal fiber. It is noteworthy to observe how it is very similar to the value of 0.6 detected by Cheng

et al. in [65] for the Kevlar fiber, through a particular micro-experimental device applied directly to a single fiber; this confirms the above noted structural analogy between sisal and aramid fibers.

Regarding, the damage mechanisms that occur under longitudinal tensile loading, the experimental evidence has shown that the tensile failure always occurs without premature appreciable debonding or fiber pull-out phenomena; it confirms both the good fiber/matrix adhesion that occurs although no surface treatment has been performed, and the absence of appreciable internal voids that can lead to a secondary debonding due to the growth of matrix defects along the matrix-fiber interface [66]. In particular, it is observed that, regardless  $V_f$ , the failure of such biocomposites occurs through failure surfaces that propagate transversally to applied load direction (see Fig.6a), followed by secondary shear local failure (failure surfaces parallel to the fiber direction) triggered by unavoidable small fiber-load alignment errors ( $3^\circ$ -  $4^\circ$ ).

However, the analysis of the SEM micrographs of the corresponding failure surfaces (see Figs.6b-e), clearly confirms the absence of debonding and pull-out phenomena. The SEM images show in fact the presence of fibers broken exactly on the fracture plane (see Figs.6b and 6c), mixed to fiber segments having length always less than the fiber diameter (see Figs.6d and 6e), i.e. less than the critical length, that for this couple of materials (sisal fiber/green epoxy) takes values no less than 2.5 mm [40, 42]; in any case no significant lateral fiber surfaces are observed.

### 3.2. Mechanical behavior under transversal tensile loading

The transversal tensile tests have shown that the examined biocomposites exhibit in practice an almost linear elastic behavior up to failure, that occurs for a mean failure strain  $\varepsilon_{T,R} = 0.27\%$  and very low failure stress  $\sigma_{T,R}$  values, that decreases from about 20 MPa to about 5.5 MPa when  $V_f$  varies from 0.2 to 0.7.

Also, the analysis of the specimens after the tests (Fig.7a) shows how the fracture is characterized by a multitude of fibers subjected to evident splitting phenomena, due to the low mutual adhesion of the sub-fibers that constitute each sisal fiber. An accurate examination shows the formation of several thin fibers produced by the splitting phenomena, typically characterized by irregular surfaces. Such splitting phenomena are widely confirmed by the analysis of SEM micrographs performed on the fracture surfaces (see Figs.7b and 7c) that show the lateral surface of fibers that have suffered evident splitting phenomena; internal transversal failures corresponding to the separation of the sub-fibers at their interface, are clearly evident. Similar splitting phenomena is also surprisingly observed during the manual manufacturing of the unidirectional stitched fabrics: two or more fibers are formed easily from an initial fiber under low accidental transversal stresses.

It is worthy to note how the observed low transversal splitting strength of the sisal fibers justifies the poor results reported in literature [45-52] about the limited failure strength improvement of random short fiber biocomposites, detected after the implementation of various surface treatments, although they seem to improve appreciably the matrix-fiber adhesion in pull-out tests. In other words, such poor results of the various fiber treatments occurs because the failure process is not governed by the matrix/fiber interface strength, but rather than by the “internal” fiber splitting phenomena, which have not been detected till now in literature.

It is also important to note that, such splitting phenomena never occur in presence of longitudinal tensile load; therefore they do not influence the pull-out strength and neither the fiber-matrix debonding strength under prevalent longitudinal tensile loading, how it has been observed in the previous section, and also widely confirmed in previous works [40, 42] that describe in detail proper pull-out test.

Taking into account the observed fiber splitting phenomenon, the transversal strength of the analyzed biocomposites can be estimated by considering the representative volume element (RVE) of the periodic microstructure model (PMM) constituted by a simple circular fiber with mean diameter  $D$ , embedded in a square matrix volume [61, 62, 67] having side  $D/L = 2 (V_f/\pi)^{1/2}$  (Figs.8a and 8b). In detail, for high  $V_f$  values (eg.  $V_f = 70\%$ ) the damage will propagate with failure surface coincident with the middle section of the RVE (Fig.8b), then the equation of the horizontal equilibrium at the incipient failure condition provides:

$$\sigma_{T,R} = \sigma_{T,R}^{(f)} \frac{D}{L} + E_m \varepsilon_{T,R} \frac{(L-D)}{L} = \sigma_{T,R}^{(f)} 2 \sqrt{\frac{V_f}{\pi}} + E_m \varepsilon_{T,R} \left( 1 - 2 \sqrt{\frac{V_f}{\pi}} \right) \quad (4)$$

In which  $\sigma_{T,R}^{(f)}$  is the fiber splitting strength, whereas  $\varepsilon_{T,R}$  is the failure strain of the unidirectional lamina under transversal tensile loading.

The experimental knowledge of the first term  $\sigma_{T,R}^{(f)}$  of Eq.(4) provided from the transversal tensile tests, permits immediately the evaluation of the unknown fiber splitting strength  $\sigma_{T,R}^{(f)}$ ; in particular, by considering the better conditioned case  $V_f=0.7$  (higher fiber volume fraction considered), which corresponds  $\varepsilon_{T,R} = 0.27\%$  and  $\sigma_{T,R} = 5.67$  MPa, (as well as  $E_m=2.5$  GPa), from Eq.(4) it follows:

$$\sigma_{T,R}^{(f)} = \left[ \sigma_{T,R} - E_m \varepsilon_{T,R} \left( 1 - 2 \sqrt{\frac{V_f}{\pi}} \right) \right] \left( 2 \sqrt{\frac{V_f}{\pi}} \right)^{-1} = 5.55 \text{ MPa} \quad (5)$$

It is seen how the sisal fiber exhibits a very high strength anisotropy, never detected until now: the longitudinal tensile strength is higher than two order of magnitude respect to the transversal one (strength anisotropy ratio  $675/4.48 \approx 150$ ).



Obviously, for low  $V_f$  values the premature fiber splitting does not lead to the biocomposite failure that is, instead, related to the matrix failure; in this condition the horizontal equilibrium equation written by considering again the RVE of the PMM (Fig.8b), provides the relationship between the biocomposite strength  $\sigma_{T,R}$  and the matrix strength:

$$\sigma_{T,R} = \sigma_{m,R} \frac{(L-D)}{L} = \sigma_{m,R} \left( 1 - 2 \sqrt{\frac{V_f}{\pi}} \right) \quad (6)$$

As it can be seen from Fig.9a, the relationship represented by Eq.(4) fits very well the experimental data for  $V_f > 0.6$ , whereas Eq.(6) fits well the experimental data for  $V_f \leq 0.6$ . The value  $V_f = 0.6$  corresponds therefore to the so called *minimum fiber volume fraction*  $V_{f,min}$  because for  $V_f \leq 0.6$  the transversal failure of the biocomposite is governed by the matrix strength, whereas for  $V_f \geq 0.6$  it is governed by the splitting strength of the fibers.

Fig.9b shows the values of transversal Young's modulus detected experimentally, along with the curve that represents the Halpin-Tsai model (red dashed line) commonly used in literature for the description of the transversal Young's modulus of unidirectional composites [61, 62], implemented in general by assuming the fiber as an isotropic material. It is seen how, unlike it commonly occurs for a generic composite reinforced by synthetic fibers, the transversal Young's modulus  $E_T$  of the examined unidirectional lamina, is not an increasing function of  $V_f$ , but it is a slightly decreasing function that does not accord at all with the classical isotropic Halpin-Tsai model.

The significant deviations observed confirms the appreciable anisotropy of the sisal fiber, not only in terms of mechanical strength, as above observed, but also in terms of elastic properties. Therefore, the correct Halpin-Tsai model have to be written by abandoned the isotropic hypothesis and by introducing the actual transversal Young's modulus  $E_T^{(f)}$  of the fibers, i.e. by using the following corrected formula:

$$E_T = E_m \frac{1 + 2\eta V_f}{1 - \eta V_f} \quad \text{with} \quad \eta = \frac{(E_T^{(f)}/E_m) - 1}{(E_T^{(f)}/E_m) + 2} \quad (7,8)$$

The experimental knowledge of the first term  $E_T$  of Eq.(7) permits the immediate evaluation of the unknown Young's modulus  $E_T^{(f)}$ ; as above, by considering the better conditioned case of  $V_f = 0.7$  (which corresponds the experimental value  $E_T = 2.19$  GPa), after solving Eq.(7) for  $E_T^{(f)}$ , it follows:

$$E_T^{(f)} = 2.07 \text{ GPa} \quad (9)$$

Such a low value indicates a high elastic anisotropy of the sisal fiber, characterized in practice by a relatively high elastic anisotropy ratio  $E_L^{(f)}/E_T^{(f)} = 40.1 / 2.07 \approx 20$ . Such a value is higher than that detected in literature [53, 57] for other natural fibers as jute (about 7) and flax (about 6); also, it is

included between the mean value exhibited by some synthetical fiber as carbon fiber (about 16) and aramid fiber (about 36).

Finally, Fig.9c shows the good accordance between the experimental values of  $v_{TL}$  detected from the transversal tensile tests performed by varying  $V_f$ , and the value provided by the well-known formula for orthotropic materials [61, 62]:

$$v_{TL}(V_f) = v_{LT}(V_f)E_T(V_f)/E_L(V_f) \quad (10)$$

being all the variables that appear at the right member already detected by the tests above described longitudinal and transverse tests. By applying this formula to the fiber, it is possible to estimate the relative minor Poisson's ratio  $v_{TL}^{(f)}$  from the values of  $v_{LT}^{(f)}$ ,  $E_T^{(f)}$  and  $E_L^{(f)}$  already detected, as:

$$v_{TL}^{(f)} = v_{LT}^{(f)} \frac{E_T^{(f)}}{E_L^{(f)}} = 0.61 \frac{2.07}{40.1} = 0.03 \quad (11)$$

The low value of the minor Poisson's ratio confirms furtherly the significant orthotropic behavior of the sisal fiber. Such characteristics have to be considered properly for accurate stress analysis in the practical applications of the biocomposites.

### 3.3. Mechanical behavior under shear loading

In order to test which of the three methods usually used for the analysis of the shear behavior of composites, as three rail shear tests, Iosipescu test and rail shear test, is more suitable for the characterization of the analyzed biocomposites, shear tests were preliminary performed by considering all the three methods above mentioned.

As it is well known, the three rail shear test method is standardized by the ASTM D 4255 / D 4255M [68] and uses relatively large rectangular specimens instrumented with a pair of electrical strain gauge (SG) or a strain gauge rosettes (SGR), as shown in Fig.10a.

The *Iosipescu* method refers instead to the ASTM D 5379 / D 5379M [69] standard and uses relatively small specimen with double V-notch (properly instrumented with a special SG) and a special purpose-built test machine (see Fig.10b); in this work a special Vishay SG (with  $b = 12$  mm) has been used.

Finally, the two-rail shear test method is described by the same ASTM D 4255 / D 4255M standard [68], and uses a rectangular specimen equal to half the specimen used by the three rail shear test (see Fig.10c).

As an example of the experimental data obtained under shear loading, Fig.10d shows the average curves  $\tau-\gamma$  detected experimentally by the three different experimental methods for the same unidirectional biocomposite having  $V_f = 0.7$ . The experimental evidence shows how the three methods give rise to different phenomena of progressive damage, thus different  $\tau-\gamma$  curves are obtained. In

particular, in the examined case the three rail shear test, that is the method most used for composites reinforced by synthetic fibers, detects an elasto-plastic curve with shear failure that is associated to a shear strength  $\tau_{LT,R} = 18.4$  MPa, which corresponds an ultimate shear strain of about 1.25% and a mean shear modulus  $G_{LT} = 1.47$  GPa.

The Iosipescu method, instead, exhibits a much more linear curve with a slight lower shear strength  $\tau_{LT,R} = 17.5$  MPa. The relatively low value of the failure shear strain (about 0.42%) is due to the observed interference phenomena between specimen and test machine; these undesired phenomena occur due to the relatively low shear stiffness of the examined biocomposites with respect to composite specimens reinforced with synthetic fibers, for which the Iosipescu method was mainly developed. Such interference phenomena do not influence significantly the failure shear stress but lead to appreciable increasing of the apparent shear modulus that assumes the value  $G_{LT} = 4.16$  GPa, that is equal to about three times the value correctly detected by the three rail shear test.

Finally, due to the stress concentration observed near the end grip, the two-rail shear test leads to a premature and progressive damaging with a significant underestimation of the failure shear stress ( $\tau_{LT,R} \approx 12$  MPa) with errors of about -35%.

In summary, it is possible to state that only the three rail shear test can be used for a reliable analysis of both shear strength and shear modulus of unidirectional biocomposites reinforced by sisal fibers. The Iosipescu method, instead, can be advantageously used only for the analysis of the shear strength  $\tau_{LT,R}$ , whereas the two rail shear test can be used only for the determination of the mean shear modulus  $G_{LT}$ .

Taking into account such considerations, the shear behavior of the analyzed biocomposites by varying  $V_f$  has been detected accurately by using the three rail shear test. The experimental results so obtained in term of  $G_{LT}$  are reported in the following Fig.11a, along with the curve that represent the isotropic Halpin-Tsai model for shear loading [61, 62], given by the following formula that assume the sisal fiber isotropic:

$$G_{LT} = G_m \frac{1+\eta V_f}{1-\eta V_f} \quad \text{with} \quad \eta = \frac{\left(\frac{G_f}{G_m}\right)^{-1}}{\left(\frac{G_f}{G_m}\right)^{-1} + 1} \quad (12,13)$$

and

$$G_f = \frac{E_L^{(f)}}{2(1 + \nu_{LT}^{(f)})} = \frac{40.1}{2(1 + 0.61)} = 12.45 \text{ GPa} \quad (14)$$

From Fig.11a it is seen how the isotropic Halpin-Tsai model represented by Eq.(12), does not match completely the experimental data: like most synthetical fiber composite, it predict an exponential increase of  $G_{LT}$  with  $V_f$ , whereas the experimental data exhibit only a slight quasi-linear increasing. Abandoning

the hypothesis of shear isotropy of the fiber and writing the Halpin-Tsai formula by assuming an

anisotropic shear modulus  $G_{LT}^{(f)}$ , i.e.:

$$G_{LT}(V_f) = G_m \frac{1 + \eta V_f}{1 - \eta V_f} \quad \text{with} \quad \eta = \frac{(G_{LT}^{(f)}/G_m) - 1}{(G_{LT}^{(f)}/G_m) + 1} \quad (15,16)$$

then the unknown value of  $G_{LT}^{(f)}$  can be been estimated by computing first the elastic ratio  $\eta$  from Eq.(15)

for a fixed value of  $V_f$  and then  $G_{LT}^{(f)}$  by solving for it Eq.(16). By considering the best conditioned case  $V_f = 0.7$  characterized by  $G_{LT} = 1.47$  GPa (see Fig.11 a), taking into account that  $G_m = 0.90$  GPa, it follows:

$$\eta = \frac{G_{LT} - G_m}{V_f(G_m + G_{LT})} = \frac{1.47 - 0.90}{0.7(0.90 + 1.47)} = 0.34 \quad (17)$$

$$G_{LT}^{(f)} = \frac{(1 + \eta)}{(1/G_m - \eta/G_m)} = \frac{1.34}{(1/0.90 - 1.34/0.90)} = 1.84 \text{ GPa} \quad (18)$$

Fig.11a shows the very good correspondence between the experimental data and the anisotropic Halpin-Tsai model described by Eq.(12); this confirm how the intimate anisotropic structure of the sisal fibers influences significantly also its shear properties and, consequently the shear behavior of the biocomposite lamina. The ratio between the isotropic  $G_f$  value given by Eq.(14) and the actual anisotropic value  $G_{LT}^{(f)}$  detected experimentally by Eqs.(17) and (18), equal to  $12.45/1.84 \approx 7$ , can be considered an index of the anisotropy of the fiber shear modulus.

The Fig.11b shows the shear strength values experimentally detected by using the three rail shear tests. It is observed how the shear strength  $\tau_{LT,R}$  of the analyzed biocomposites is not a monotonic function of the fiber volume fraction, but it decreases for low value of  $V_f$  and increases for high  $V_f$  values. This results indicate that for low  $V_f$  values the shear failure of the biocomposite corresponds to the matrix failure that occurs after the fiber failure, whereas for high values of  $V_f$  it corresponds to the fiber failure, which follows immediately the matrix. Consequently, for low fiber volume fraction the  $\tau_{LT,R}$  is related only to the matrix shear strength  $\tau_{m,R}$  by the following simple relationship:

$$\tau_{LT,R} = \tau_{m,R} V_m \quad (19)$$

For high fiber volume fraction, instead, the shear strength  $\tau_{LT,R}$  is given by the sum of the contribution of the fiber (at the incipient failure condition in which  $\tau_{LT}^{(f)} = \tau_{LT,R}^{(f)}$ ) and the contribution of the matrix by the following formula:

$$\tau_{LT,R} = \tau_{LT,R}^{(f)} V_f + \tau_m^* V_m = \tau_{LT,R}^{(f)} \left( V_f + \frac{V_m}{k_\tau} \right) \quad (20)$$

where  $\tau_m^*$  is the shear stress acting to the matrix at the incipient failure condition of the fiber ( $\tau_{LT}^{(f)} = \tau_{LT,R}^{(f)}$ ),

whereas  $k_\tau = \tau_{LT,R}^{(f)} / \tau_m^*$  is the shear stress concentration factor due to the shear stiffness mismatch between

fiber ( $G_{LT}^{(f)}=1.84$  GPa) and matrix ( $G_m=0.9$  GPa). By solving the equation system obtained by written Eq.(20) for two different  $V_f$  values it is possible first to evaluate the unknown values of  $\tau_{LT,R}^{(f)}$  and  $k_\tau$ . As an example, by considering  $V_f = 0.4$  and  $V_f=0.7$ , it follows:

$$k_\tau=1.29 \quad \text{and} \quad \tau_{LT,R}^{(f)} = 19.8 \text{ MPa} \quad (21,22)$$

It is important to note how, unlike composites reinforced by synthetic fibers, the value of the shear strength of the fiber (19.8 MPa) is lower than that of the matrix (25 MPa) and consequently, the sisal fibers do not contribute to improve the matrix shear strength. From Fig.11b it is seen that both Eqs.(19) and (20) are in a good accordance with the experimental data; also, their graphical intersection indicates that in practice in this case the transition fiber volume fraction  $V_{f,min} \approx 0.3$ .

Finally, concerning the damaging processes under shear loading, the experimental evidence has shown that, like laminae reinforced by synthetic fibers, the shear failure occurs with typical failure surface parallel to the fiber direction. In more detail, the analysis of the SEM micrographic images (see Fig.12) shows how the shear damage process always involves fiber shear failure that consists on internal separation of the sub-fibers (shear splitting); unlike the transversal loading case, now the surface of the damaged sub-fibers appears more irregular because the failure surface due to shear loading does not follows exactly the sub-fibers surface, as instead occurs in the case of transversal tensile loading (see Figs.7b and 7c).

#### 3.4. Mechanical behavior under longitudinal compressive loading

The experimental tests have shown that under longitudinal compressive loading the examined biocomposites exhibits an elastic behavior with a compressive longitudinal Young's modulus  $E'_L$  that decreases progressively with the applied load. As an example Fig.13a show the compressive curves detected by the specimens having  $V_f=0.5$ ; similar curve have been obtained for the other  $V_f$  values considered. Such a decreasing can be reasonably due to the buckling of the fibers; in more detail, it is seen how  $E'_L$  starts with a value that coincides with the tensile longitudinal modulus  $E_L$  and tends to zero when the applied longitudinal compressive stress  $\sigma'_L$  tends to the corresponding failure value  $\sigma'_{L,R}$  that is associated by a relatively low longitudinal failure strain  $\varepsilon'_{L,R} \approx 0.6$  % ; the experimental evidence show that this last value is quite constant also by varying  $V_f$ . Also, the experimental results shows that in practice the elastic ratio  $R_E = E'_L/E_L$  is a function of  $V_f$  and of the load ratio  $\sigma'_L/\sigma'_{L,R}$ , and is well fitted by the following empirical formula obtained by interpolating the experimental results:

$$R_E = E'_L/E_L = 1 + \left( \sqrt{\frac{1}{10(1-V_f)}} - 1 \right) \left[ 1.35 \left( \frac{\sigma'_L}{\sigma'_{L,R}} \right)^2 - 0.54 \left( \frac{\sigma'_L}{\sigma'_{L,R}} \right) \right] \quad (23)$$

Taking into account the expression of  $E_L$  given by Eq.(2), Eq.(23) allows the user the evaluation of the compressive longitudinal Young's modulus by the following re-arranged expression:

$$E'_L = [E_L^{(f)}V_f + E_m(1 - V_f)] \left\{ 1 + \left( \sqrt{\frac{1}{10(1 - V_f)}} - 1 \right) \left[ 1.35 \left( \frac{\sigma'_L}{\sigma'_{L,R}} \right)^2 - 0.54 \left( \frac{\sigma'_L}{\sigma'_{L,R}} \right) \right] \right\} \quad (24)$$

Regarding the compressive strength, the experimental evidence has shown that the limited values of the failure strain  $\varepsilon'_{L,R}$  (about 0.6%) are always associated with a transversal failure (due to the transverse strain) that occurs with typical longitudinal fracture surfaces, as it is clearly shown in the following Fig.13b that depicts a specimens after the longitudinal compressive test. The longitudinal compressive strength  $\sigma'_{L,R}$  is therefore strictly related to the low transversal failure strain  $\varepsilon_{T,R}$  associated to the fiber splitting phenomena above detected in section 3.2. Taking into account the Poisson's effect that links longitudinal and the transversal strain, the well-known micromechanical relationships that relate the longitudinal Young's modulus and the Poisson's ratio with the elastic properties of the constituent materials, as well as the ratio  $R_E$  provided by Eq.(23), then the compressive strength  $\sigma'_{L,R}$  can be described by the well-known following formula [61, 62]:

$$\varepsilon'_{L,R} = -\frac{\varepsilon_{T,R}}{\nu_{LT}} \rightarrow \sigma'_{L,R} = E'_L \varepsilon'_{L,R} = -\frac{E'_L \varepsilon_{T,R}}{\nu_{LT}} = -\frac{R_E(E_L^{(f)}V_f + E_mV_m)}{(\nu_{LT,f}V_f + \nu_mV_m)E_T} \sigma_{T,R} \quad (25)$$

By substituting  $\sigma_{T,R}$  by Eq.(4) and by Eq.(6) respectively for  $V_f$  higher and lower to 0.6 (see Fig.9a), Eq.(25) became:

$$\sigma'_{L,R} = \begin{cases} -\frac{R_E(E_L^{(f)}V_f + E_mV_m)}{(\nu_{LT,f}V_f + \nu_mV_m)E_T} \sigma_{m,R} \left( 1 - 2\sqrt{\frac{V_f}{\pi}} \right) & \text{for } V_f \leq 0.6 \\ -\frac{2R_E(E_L^{(f)}V_f + E_mV_m)}{(\nu_{LT,f}V_f + \nu_mV_m)E_T} \sigma_{T,R}^{(f)} \sqrt{\frac{V_f}{\pi}} + E_m \varepsilon_{T,R} \left( 1 - 2\sqrt{\frac{V_f}{\pi}} \right) & \text{for } V_f > 0.6 \end{cases} \quad (26,27)$$

Fig.13c shows the good agreement between the experimental data obtained from the longitudinal compressive tests and the theoretical prediction of the longitudinal compressive strength expressed by Eq.(26) and (27) (deviations lower than a few percentage points). It is important to observe how, due to the opposite effects of the  $V_f$  increasing on the longitudinal stiffness (positive) and on the transversal strength (negative due to the low transverse fiber strength, see section 3.2), the longitudinal compressive strength of the unidirectional biocomposite laminae increases with  $V_f$  if the fiber volume fraction falls in the range  $0 < V_f < 0.3$ , whereas it decreases for  $0.3 \leq V_f \leq 0.6$ ; finally it increases again slightly for  $V_f > 0.6$ . Synthetically, it is possible to state that for the common values of  $V_f$  used for structural composites ( $0.3 \leq V_f \leq 0.7$ ), like the transversal tensile strength, the longitudinal compressive strength does not benefit from the increment of fiber volume fraction; in practice the maximum longitudinal compressive strength corresponds to  $V_f = 0.3$  and is equal to about 100 MPa (see Fig.13c).

Furthermore, taking into account that in absence of buckling phenomena (low compressive loads) the compressive Young's modulus of the biocomposite is equal to the tensile one, as well as that its decreasing is related only to the buckling phenomena, it is possible to state that the compressive stiffness of the sisal fiber is equal to the tensile one, i.e.  $E_L^{(f)} = E_L^{(f)}$ .

### 3.5. Mechanical behavior under transversal compressive loading

The experimental evidence has shown that, like longitudinal compressive case, also for transversal compressive loading the failure of the examined biocomposites occurs for transversal tensile (see Fig.14a). This particular damage process indicates that the transversal compressive failure occurs in practice when the compressive strain  $\varepsilon'_{T,R}$  (parallel to the applied load) reaches the ultimate values  $\varepsilon'_{T,R}$  that is related to the ultimate tensile strain  $\varepsilon_{T,R}$  (orthogonal to the lamina) by the following simple relationship:

$$\varepsilon'_{T,R} = -\frac{\varepsilon_{T,R}}{\nu_{TT}} \rightarrow \sigma'_{T,R} = -\frac{E_T \varepsilon_{T,R}}{\nu_{TT}} = -\frac{\sigma_{T,R}}{\nu_{TT}} \quad (28,29)$$

where  $\sigma'_{T,R}$  and  $\nu_{TT}$  are the searched compressive strength and the transversal Poisson's ratio of the examined unidirectional lamina, respectively. Taking into account the transversal isotropy of the unidirectional lamina, by substituting  $\sigma_{T,R}$  with Eq.(4) or Eq.(6), and  $\nu_{TT}$  by the formula given by the well-known Compliance Averaging Model [67]:

$$\frac{\nu_{TT}}{E_T} = \left( \frac{\nu_{TT}^{(f)}}{E_T^{(f)}} \right) V_f + \left( \frac{\nu_m}{E_m} \right) V_m \quad (30)$$

then Eq.(29) can be rewritten as:

$$\sigma'_{T,R} = -\frac{\sigma_{T,R}}{\nu_{TT}} = -\frac{1}{\frac{\nu_{TT}^{(f)} V_f}{E_T^{(f)}} + \frac{\nu_m V_m}{E_m}} \begin{cases} \sigma_{m,R} \left( 1 - 2\sqrt{\frac{V_f}{\pi}} \right) & \text{for } V_f \leq 0.6 \\ \sigma_{T,R}^{(f)} 2\sqrt{\frac{V_f}{\pi}} + E_m \varepsilon_{T,R} \left( 1 - 2\sqrt{\frac{V_f}{\pi}} \right) & \text{for } V_f > 0.6 \end{cases} \quad (31,32)$$

The unknown Poisson's ratio  $\nu_{TT}^{(f)}$  can be computed by solving these equations for this parameter; as an example, by solving Eq.(32) for the case best conditioned case of the biocomposite lamina having  $V_f = 0.7$ , which corresponds the experimental value  $\sigma'_{T,R} = 19.55$  MPa (compressive test), the following value is computed:

$$\nu_{TT}^{(f)} = 0.21 \quad (33)$$

It is noteworthy to observe as this value is very near the transversal Poisson's ratio of various anisotropic and isotropic fibers, as the Kevlar KM2 fiber having  $\nu_{TT}^{(f)} = 0.24$  [64] and glass fiber having commonly  $\nu_{TT}^{(f)} = 0.22$  [61, 62].

Fig.14b shows the transversal compressive strength  $\sigma'_{T,R}$  detected experimentally by varying  $V_f$ , along with the curves that represent Eq.(31) and Eq.(32). It is seen how the transversal compressive strength is accurately fitted by this equations for  $V_f \leq 0.6$  and for  $V_f > 0.6$  respectively (deviations always less than about 8%). Also, the comparison between Figs.13c and 14b shows that, for any fixed  $V_f$  value, the longitudinal compressive strength, that benefits by the high longitudinal stiffness of the fibers, is always appreciably higher than the transversal compressive one. However, like most composites reinforced by synthetical fibers, this last assumes values (from 70 MPa to 20 MPa, see Fig.14b) that for a fixed  $V_f$  value, are about 3÷4 times higher than the transversal tensile strength (from 20 MPa to 5 MPa, see Fig.9a).

Regarding the transversal compressive Young's modulus  $E'_T$ , the experimental evidence has shown that in practice for any  $V_f$  value, it coincides with the tensile one, i.e.  $E'_T \approx E_T$ . Consequently, from such a result it is possible to state that, similarly to the longitudinal case, also the transversal compressive Young's modulus of the fiber is in practice equal to the tensile one, i.e.  $E_T^{(f)} \approx E_T^{(f)}$ .

Finally, it is possible to state that the above exposed experimental results have shown clearly the high anisotropy of the sisal fiber in term of both elastic properties and mechanical strength, as well as its noticeably influence on the mechanical behavior of the corresponding high-performance unidirectional biocomposite lamina that can be used for the implementation of green laminates for practical structural applications. In detail, due to the detected splitting phenomena, the transversal and the shear mechanical properties of the fiber are both relatively low. Consequently, except the longitudinal tensile case in which the unidirectional lamina exhibits high mechanical performance comparable with that of a GFRP, under all the other loading conditions (included longitudinal and transversal compressive) its strength is instead significantly limited by the low splitting strength of the fiber. Consequently, if for a fixed loading condition the lay-up of the biocomposite laminate leads to transversal or shear damage mechanisms, then a very limited strength is expected. As an example, it is the case of the common randomly short fiber biocomposites whose damage process involve always transversal and/or shear damage mechanisms. In the opinion of the authors the low transversal strength is a common feature of the most natural fibers, and it explains why all the surface treatments of the fibers do not lead to appreciable strength improvements of the reinforced biocomposites, which can be enhancements only by proper treatments able to improve the (internal) mutual sub-fibres adhesion.

#### 4. CONCLUSIONS

Through a systematic experimental test campaign, carried out on high performance unidirectional laminae constituted by green epoxy reinforced by sisal fibers, it has been highlighted how, in accordance with its non-isotropic internal structure constituted by a multitude of hollow cylindrical sub-fibers, the



sisal fiber exhibits an orthotropic transversally isotropic behavior in terms of both elastic properties and mechanical strength.

In detail, as it is shown in Tab.1, the transversal Young's modulus  $E_T^{(f)}$  is about 1/20 the longitudinal one  $E_L^{(f)}$ , and the actual shear modulus  $G_{LT}^{(f)}$  is about 1/7 the isotropic one estimable by assuming a shear isotropic behavior; also, the actual major Poisson's ratio  $\nu_{LT}^{(f)}$  falls out the isotropic range  $0 \div 0.5$ . In the transversal section, instead, the Poisson's ratio  $\nu_{TT}^{(f)}$  is very close to the values of most synthetical fibers (kevlar, glass etc.). However, in both longitudinal and transversal direction the fiber exhibits a symmetrical behavior, i.e. the compressive Young's moduli  $E_L'^{(f)}$  and  $E_T'^{(f)}$  are equal to the corresponding tensile ones  $E_L^{(f)}$  and  $E_T^{(f)}$  (Tab.1).

Concerning instead the mechanical strength of the fiber (see Tab.2), due to the fiber splitting phenomena clearly evidenced by the experimental tests and widely confirmed by SEM micrographs, the transversal tensile strength  $\sigma_{T,R}^{(f)}$  is more than two order of magnitude lower than the longitudinal one  $\sigma_{L,R}^{(f)}$ . Due to the same damage process (fiber splitting), also the actual fiber shear strength  $\tau_{LT,R}^{(f)}$  is quite low (see Tab.2).

The compressive tests carried out in both longitudinal and transversal direction, have not permitted to detect the corresponding strengths  $\sigma_{L,R}'^{(f)}$  and  $\sigma_{T,R}'^{(f)}$  of the fiber because under such loading conditions the failure of the unidirectional laminae occurs always by the transversal tensile damaging, related to the low fiber splitting strength  $\sigma_{T,R}^{(f)}$ . Obviously, such a lack of knowledge does not limit the prediction of the laminate biocomposites strength in practical applications, because in accordance with the experimental evidence, the biocomposite failure never involves compressive failure of the fiber.

Such an anisotropic properties of the sisal fiber are described reliable micromechanical models properly incremented; they can be used advantageously (at the design stage) for the prediction of the mechanical behavior of the unidirectional lamina, by varying the fiber volume fraction. In detail, as it is presented in Tab.3, both the longitudinal Young's modulus  $E_L$  and the major Poisson's ratio  $\nu_{LT}$  obey the rule of mixture, whereas the transversal Young's modulus  $E_T$  is well fitted by an anisotropic Halpin-Tsai model that involves the actual transverse Young's modulus  $E_T^{(f)}$ ; also the shear modulus  $G_{LT}$  is described accurately by the Halpin-Tsai model if the detected anisotropic shear modulus of the fiber  $G_{LT}^{(f)}$  is properly introduced. The transversal Poisson's ratio  $\nu_{TT}$  instead is well described by the compliance averaging model. Also, regarding the compressive behavior, the experimental evidence has shown that the compressive transversal modulus  $E_T'$  coincides in practice with the tensile one  $E_T$  whereas, due to

unavoidable fiber buckling, the longitudinal compressive Young's modulus  $E'_L$  exhibits an appreciable reduction respect to the tensile one  $E_L$ ; such a progressive reduction is accurately described by a simple ratio  $R_E = E'_L / E_L$  whose theoretical formula has been properly developed from the observed experimental results.

Finally, concerning the mechanical strength of the unidirectional laminae, as it is exposed in Tab.4, the experimental analysis has shown that the longitudinal tensile strength  $\sigma_{L,R}$  obeys the rule of mixture with a corrective factor of about 0.85 that takes into account all the influence parameters (fiber damage during biocomposite manufacturing, fiber misalignment etc.); accurate predictions of the transversal tensile strength  $\sigma_{T,R}$  and the shear strength  $\tau_{LT,R}$ , are provided instead by a proper micromechanical model developed from the PMM model by considering the actual low splitting strength experimentally detected. Regarding both the longitudinal and transversal compressive strength, two corresponding accurate micromechanical models have been implemented by relating the ultimate compressive stresses  $\sigma'_{L,R}$  and  $\sigma'_{T,R}$  with the ultimate transversal strain  $\varepsilon_{T,R}$  given by the PMM.

## ACKNOWLEDGEMENTS

This work was supported by the MISE [grant number F/050162/02/X32].

## REFERENCES

- [1] Ahmad F, Choi HS, Park MK. A review: Natural fiber composites selection in view of mechanical, light weight, and economic properties. *Macromol Mater Eng* 2015;300:10–24. <https://doi.org/10.1002/mame.201400089>.
- [2] Li Y, Mai Y, Ye L. Sisal fibre and its composites : a review of recent developments IM PA US AS DO ME US EX ON AS. *Compos Sci Technol* 2000;60:2037–55.
- [3] Omrani E, Menezes PL, Rohatgi PK. State of the art on tribological behavior of polymer matrix composites reinforced with natural fibers in the green materials world. *Eng Sci Technol an Int J* 2016;19:717–36. <https://doi.org/10.1016/j.jestch.2015.10.007>.
- [4] Koronis G, Silva A, Fontul M. Green composites: A review of adequate materials for automotive applications. *Compos Part B Eng* 2013;44:120–7. <https://doi.org/10.1016/j.compositesb.2012.07.004>.
- [5] Nabi Saheb D, Jog JP. Natural fiber polymer composites: A review. *Adv Polym Technol* 1999;18:351–63. [https://doi.org/10.1002/\(SICI\)1098-2329\(199924\)18:4<351::AID-ADV6>3.0.CO;2-X](https://doi.org/10.1002/(SICI)1098-2329(199924)18:4<351::AID-ADV6>3.0.CO;2-X).
- [6] Ku H, Wang H, Pattarachaiyakoo N, Trada M. A review on the tensile properties of natural fiber reinforced polymer composites. *Compos Part B Eng* 2011;42:856–73. <https://doi.org/10.1016/j.compositesb.2011.01.010>.
- [7] Jagadeesh D, Kanny K, Prashantha K. A Review on Research and Development of Green Composites From Plant Protein-Based Polymers. *Polym Compos* 2017;37:915–24. <https://doi.org/10.1002/pc>.
- [8] Bharath KN, Basavarajappa S. Applications of biocomposite materials based on natural fibers from renewable resources: A review. *Sci Eng Compos Mater* 2016;23:123–33. <https://doi.org/10.1515/secm-2014-0088>.

- [9] Ramesh M, Palanikumar K, Reddy KH. Plant fibre based bio-composites: Sustainable and renewable green materials. *Renew Sustain Energy Rev* 2017;79:558–84. <https://doi.org/10.1016/j.rser.2017.05.094>.
- [10] Shekar HSS, Ramachandra M. Green Composites: A Review. *Mater Today Proc* 2018;5:2518–26. <https://doi.org/10.1016/j.matpr.2017.11.034>.
- [11] Benzait Z, Trabzon L. A review of recent research on materials used in polymer–matrix composites for body armor application. *J Compos Mater* 2018;52:3241–63. <https://doi.org/10.1177/0021998318764002>.
- [12] Sanjay MR, Madhu P, Jawaidd M, Sentharamaikannan P, Senthil S, Pradeep S. Characterization and properties of natural fiber polymer composites: A comprehensive review. *J Clean Prod* 2018;172:566–81. <https://doi.org/10.1016/j.jclepro.2017.10.101>.
- [13] Khan T, Hameed Sultan MT Bin, Ariffin AH. The challenges of natural fiber in manufacturing, material selection, and technology application: A review. *J Reinf Plast Compos* 2018;37:770–9. <https://doi.org/10.1177/0731684418756762>.
- [14] Mohammed L, Ansari MNM, Pua G, Jawaidd M, Islam MS. A Review on Natural Fiber Reinforced Polymer Composite and Its Applications. *Int J Polym Sci* 2015;2015:15. <https://doi.org/10.1155/2015/243947>.
- [15] Nunna S, Chandra PR, Shrivastava S, Jalan AK. A review on mechanical behavior of natural fiber based hybrid composites. *J Reinf Plast Compos* 2012;31:759–69. <https://doi.org/10.1177/0731684412444325>.
- [16] Di Landro L, Janszen G. Composites with hemp reinforcement and bio-based epoxy matrix. *Compos Part B Eng* 2014;67:220–6. <https://doi.org/10.1016/j.compositesb.2014.07.021>.
- [17] Hong CK, Wool RP. Development of a Bio-Based Composite Material from Soybean Oil and Keratin Fibers. *J Appl Polym Sci* 2005;95:1524–38. <https://doi.org/10.1002/app.21044>.
- [18] Haq M, Burgueño R, Mohanty AK, Misra M. Hybrid bio-based composites from blends of unsaturated polyester and soybean oil reinforced with nanoclay and natural fibers. *Compos Sci Technol* 2008;68:3344–51. <https://doi.org/10.1016/j.compscitech.2008.09.007>.
- [19] Feldmann M, Bledzki AK. Bio-based polyamides reinforced with cellulosic fibres – Processing and properties. *Compos Sci Technol* 2014;100:113–20. <https://doi.org/10.1016/j.compscitech.2014.06.008>.
- [20] Patel M, Bastioli C, Marini L, Wurdinger E. Life- cycle Assessment of Bio- based Polymers and Natural Fiber Composites. *Biopolymers* 2005;10. <https://doi.org/10.1002/3527600035.bpola014>.
- [21] Satyanarayana KG, Arizaga GGC, Wypych F. Biodegradable composites based on lignocellulosic fibers — An overview. *Prog Polym Sci* 2009;34:982–1021. <https://doi.org/10.1016/j.progpolymsci.2008.12.002>.
- [22] Yan L, Kasal B, Huang L. A review of recent research on the use of cellulosic fibres, their fibre fabric reinforced cementitious, geo-polymer and polymer composites in civil engineering. *Compos Part B Eng* 2016;92:94–132. <https://doi.org/10.1016/j.compositesb.2016.02.002>.
- [23] Dicker MPM, Duckworth PF, Baker AB, Francois G, Hazzard MK, Weaver PM. Green composites: A review of material attributes and complementary applications. *Compos Part A Appl Sci Manuf* 2014;56:280–9. <https://doi.org/10.1016/j.compositesa.2013.10.014>.
- [24] Mohanty AK, Manjusri M, Drzal LT. *Natural Fibers , Biopolymers , and Biocomposites*. CRC Press. 2005.
- [25] Faruk O, Bledzki AK, Fink HP, Sain M. Biocomposites reinforced with natural fibers: 2000–2010. *Prog Polym Sci* 2012;37:1552–96. <https://doi.org/10.1016/j.progpolymsci.2012.04.003>.

- [26] Langhorst AE, Burkholder J, Long J, Thomas R, Kiziltas A, Mielewski D. Blue-Agave Fiber-Reinforced Polypropylene Composites for Automotive Applications. *BioresourcesCom* 2018;13:820–35.
- [27] Sreekumar PA, Joseph K, Unnikrishnan G, Thomas S. A comparative study on mechanical properties of sisal-leaf fibre-reinforced polyester composites prepared by resin transfer and compression moulding techniques. *Compos Sci Technol* 2007;67:453–61. <https://doi.org/10.1016/j.compscitech.2006.08.025>.
- [28] Murherjee P, Satyananarayana K. Structure and properties of some vegetable fibres, part. 1 Sisal Fibres. *J Mater Sci* 1986;19:3925–6.
- [29] Chand N, Hashmi SAR. Mechanical properties of sisal fibre at elevated temperatures. *J Mater Sci* 1993;28:6676–82. <https://doi.org/10.1007/BF00356422>.
- [30] Chand N, Verma S, Khazanchi AC. SEM and strength characteristics of acetylated sisal fibre. *J Mater Sci Lett* 1989;8:1307–9. <https://doi.org/10.1007/BF00721503>.
- [31] Silva F de A, Chawla N, Filho RD de T. Tensile behavior of high performance natural (sisal) fibers. *Compos Sci Technol* 2008;68:3438–43. <https://doi.org/10.1016/j.compscitech.2008.10.001>.
- [32] Thomason JL, Carruthers J, Kelly J, Johnson G. Fibre cross-section determination and variability in sisal and flax and its effects on fibre performance characterisation. *Compos Sci Technol* 2011;71:1008–15. <https://doi.org/10.1016/j.compscitech.2011.03.007>.
- [33] Belaadi A, Bezazi A, Bourchak M, Scarpa F, Zhu C. Thermochemical and statistical mechanical properties of natural sisal fibres. *Compos Part B Eng* 2014;67:481–9. <https://doi.org/10.1016/j.compositesb.2014.07.029>.
- [34] Milanese AC, Cioffi MOH, Voorwald HJC. Thermal and mechanical behaviour of sisal/phenolic composites. *Compos Part B Eng* 2012;43:2843–50. <https://doi.org/10.1016/j.compositesb.2012.04.048>.
- [35] Towo AN, Ansell MP. Fatigue evaluation and dynamic mechanical thermal analysis of sisal fibre-thermosetting resin composites. *Compos Sci Technol* 2008;68:925–32. <https://doi.org/10.1016/j.compscitech.2007.08.022>.
- [36] Belaadi A, Bezazi A, Maache M, Scarpa F. Fatigue in sisal fiber reinforced polyester composites: Hysteresis and energy dissipation. *Procedia Eng* 2014;74:325–8. <https://doi.org/10.1016/j.proeng.2014.06.272>.
- [37] Bezazi A, Belaadi A, Bourchak M, Scarpa F, Boba K. Novel extraction techniques, chemical and mechanical characterisation of *Agave americana* L. natural fibres. *Compos Part B Eng* 2014;66:194–203. <https://doi.org/10.1016/j.compositesb.2014.05.014>.
- [38] Zuccarello B. Static and dynamic mechanical properties of eco-friendly polymer composites. In: Inamuddin, Thomas S, Kumar Mishra R, Asiri A, editors. *Sustain. Polym. Compos. Nanocomposites* Springer Nat., Springer, Cham; 2019, p. 259–92. [https://doi.org/10.1007/978-3-030-05399-4\\_9](https://doi.org/10.1007/978-3-030-05399-4_9).
- [39] Zuccarello B, Zingales M. Toward high performance renewable agave reinforced biocomposites: Optimization of fiber performance and fiber-matrix adhesion analysis. *Compos Part B Eng* 2017;122:109–20. <https://doi.org/10.1016/j.compositesb.2017.04.011>.
- [40] Zuccarello B, Scaffaro R. Experimental analysis and micromechanical models of high performance renewable agave reinforced biocomposites. *Compos Part B Eng* 2017;119:141–52. <https://doi.org/10.1016/j.compositesb.2017.03.056>.
- [41] Zuccarello B, Marannano G, Mancino A. Optimal manufacturing and mechanical characterization of high performance biocomposites reinforced by sisal fibers. *Compos Struct* 2018;194:575–83. <https://doi.org/10.1016/j.compstruct.2018.04.007>.
- [42] Zuccarello B, Marannano G. Random short sisal fiber biocomposites: Optimal manufacturing process and reliable theoretical models. *Mater Des* 2018;149:87–100. <https://doi.org/10.1016/j.matdes.2018.03.070>.

- [43] Pantano A, Zuccarello B. Numerical model for the characterization of biocomposites reinforced by sisal fibres. *Procedia Struct Integr* 2018;8:517–25. <https://doi.org/10.1016/j.prostr.2017.12.051>.
- [44] Mancino A, Marannano G, Zuccarello B. Implementation of eco-sustainable biocomposite materials reinforced by optimized agave fibers. *Procedia Struct Integr* 2018;8:526–38. <https://doi.org/10.1016/j.prostr.2017.12.052>.
- [45] Kaewkuk S, Sutapun W, Jarukumjorn K. Effects of interfacial modification and fiber content on physical properties of sisal fiber/polypropylene composites. *Compos Part B Eng* 2013;45:544–9. <https://doi.org/10.1016/j.compositesb.2012.07.036>.
- [46] Bisanda ETN, Ansell MP. The effect of silane treatment on the mechanical and physical properties of sisal-epoxy composites. *Compos Sci Technol* 1991;41:165–78. [https://doi.org/10.1016/0266-3538\(91\)90026-L](https://doi.org/10.1016/0266-3538(91)90026-L).
- [47] Joseph K, Thomas S, Pavithran C. Effect of chemical treatment on the tensile properties of short sisal fibre-reinforced polyethylene composites. *Polymer (Guildf)* 1996;37:5139–49. [https://doi.org/10.1016/0032-3861\(96\)00144-9](https://doi.org/10.1016/0032-3861(96)00144-9).
- [48] Singh B, Gupta M, Verma A. Influence of Fiber Surface Treatment on the Properties of Sisal-Polyester Composites. *Polym Compos* 1996;17:910–8. <https://doi.org/10.1002/pc.10684>.
- [49] Mysamy K, Rajendran I. Influence of alkali treatment and fibre length on mechanical properties of short Agave fibre reinforced epoxy composites. *Mater Des* 2011;32:4629–40. <https://doi.org/10.1016/j.matdes.2011.04.029>.
- [50] Kim JT, Netravali AN. Mercerization of sisal fibers: Effect of tension on mechanical properties of sisal fiber and fiber-reinforced composites. *Compos Part A Appl Sci Manuf* 2010;41:1245–52. <https://doi.org/10.1016/j.compositesa.2010.05.007>.
- [51] Ramzy A, Beermann D, Steuernagel L, Meiners D, Ziegmann G. Developing a new generation of sisal composite fibres for use in industrial applications. *Compos Part B Eng* 2014;66:287–98. <https://doi.org/10.1016/j.compositesb.2014.05.016>.
- [52] Li Y, Ma H, Shen Y, Li Q, Zheng Z. Effects of resin inside fiber lumen on the mechanical properties of sisal fiber reinforced composites. *Compos Sci Technol* 2015;108:32–40. <https://doi.org/10.1016/j.compscitech.2015.01.003>.
- [53] Cichocki Jr. FR, Thomason JL. Thermoelastic anisotropy of a natural fiber. *Compos Part B Eng* 2002;62:669–78. [https://doi.org/10.1016/S0266-3538\(02\)00011-8](https://doi.org/10.1016/S0266-3538(02)00011-8).
- [54] Thomason JL. Dependence of Interfacial Strength on the Anisotropic Fiber Properties of Jute Reinforced Composites. *Polym Compos* 2010;39:1525–34. <https://doi.org/10.1002/pc.20939>.
- [55] Gassan J, Chate A, Bledzki AK. Calculation of elastic properties of natural fibers. *J Mater Sci* 2001;36:3715–20. <https://doi.org/10.1023/A:1017969615925>.
- [56] Ntenga R, Béakou A, Atéba J, Ohandja L. Estimation of the elastic anisotropy of sisal fibres by an inverse method. *J Mater Res Technol* 2008;43:6206–13. <https://doi.org/10.1007/s10853-008-2925-2>.
- [57] Thomason J, Yang L, Gentles F. Characterisation of the Anisotropic Thermoelastic Composite Reinforcement. *Fibers* 2017;5:36. <https://doi.org/10.3390/fib5040036>.
- [58] Kalaprasad G, Joseph K, Thomas S, Pavithran C. Theoretical modelling of tensile properties of short sisal fibre-reinforced low-density polyethylene composites. *J Mater Sci* 1997;32:4261–7. <https://doi.org/10.1023/A:1018651218515>.
- [59] Technical Data Sheet INH Hardener with Super Sap CLR system. Clear, UV Stable Infusion/RTM System. n.d.
- [60] ASTM D3822/D3822M-14. Standard Test Method for Tensile Properties of Single Textile Fibers. 2001.

- [61] Agarwal BD, Broutman LJ, Chandrashekhara K. Analysis and performance of fiber composites. New Delhi: John Wiley & Sons; 1998.
- [62] Barbero EJ. Introduction to composite materials design. New York: Taylo & Francis Group; 1999.
- [63] ASTM D3039/D3039M-00. Standard Test Method for Tensile Properties of Polymer Matrix Composite Materials. 2002.
- [64] ASTM D6641/D6641M-09. Standard Test Method for Compressive Properties of Polymer Matrix Composite Materials Using a Combined Loading Compression ( CLC ) Test Fixture. 2014.
- [65] Cheng M, Chen W, Weerasooriya T. Mechanical Properties of Kevlar® KM2 Single Fiber. J Eng Mater Technol 2005;127:197–203. <https://doi.org/10.1115/1.1857937>.
- [66] Cirello A, Zuccarello B. On the effects of a crack propagating toward the interface of a bimaterial system. Eng Fract Mech 2006;73:1264–77. <https://doi.org/10.1016/j.engfracmech.2005.12.003>.
- [67] Bogdanovich A, Pastore C. Mechanics of Textile and Laminated Composites. London: Chapman & Hall; 1996.
- [68] ASTM D4255/D4255M-01. Standard Test Method for In-Plane Shear Properties of Polymer Matrix Composite Materials by the Rail Shear Method. 2007.
- [69] ASTM D5379/D5379M-19. Standard Test Method for Shear Properties of Composite Materials by the V-Notched Beam Method. 2019.

## FIGURE CAPTIONS

**Fig.1.** (a) plants of agave sisalana, (b) fibers, (c) typical horseshoe fiber section and (d) hollow cylindrical sub-fibers.

**Fig.2.** Unidirectional stitched fabric made on laboratory: (a) alignment and stretching of the fibers,(b) fabric after transversal stitching.

**Fig.3.** Biocomposite manufacturing: (a) hand lay-up inside the mold, (b) mold, counter-mold and press used for the thermo-mechanical compression moulding and (c) biocomposite panel obtained.

**Fig.4.** Longitudinal and transverse tensile tests performed by using an INSTRON 3367 material test machine and specimens instrumented by a micrometer type HBM and a transversal ER type VISHAY.

**Fig. 5.** (a) Longitudinal tensile strength and theoretical ROM models represented by Eq.1; (b) longitudinal Young's modulus and theoretical model represented by Eq.(2); (c) major Poisson's ratio and theoretical model given by Eq.(3a).

**Fig.6.** (a) Typical image of specimens fractured by tensile test and (b-e) SEM micrographs of the corresponding fracture surfaces.

**Fig.7.** (a) Typical image the specimens after transversal tensile test and (b, c) SEM micrographs of the fracture surfaces that evidence the fiber splitting.

**Fig.8.** PMM: (a) typical model scheme and (b) RVE used for the analysis of the transversal tensile strength.

**Fig.9.** (a) Transversal tensile strength and theoretical models obtained by PMM; (b) transverse Young's modulus and Halpin-Tsai models; (c) minor Poisson ratio  $\nu_{TL}$  and model provided by micromechanics.

**Fig.10:** Shear tests: (a) three rail shear test, (b) Iosipescu shear test, (c) two rail shear test and (d) mean shear curves relative to the unidirectional lamina biocomposite with  $V_f = 70\%$ .

**Fig.11:** (a) Shear modulus of the analyzed biocomposite laminae versus  $V_f$  and Halpin-Tsai models; (b) shear strength versus  $V_f$  and theoretical models proposed.

**Fig.12:** SEM micrographs of the fracture surface of the analyzed specimens under shear loading, showing the typical internal fiber splitting.

**Fig.13:** (a) typical longitudinal compressive curves for the biocomposite examined ( $V_f = 0.5$ ); (b) typical transversal tensile failure; (c) longitudinal compressive strength vs.  $V_f$  and theoretical models given by Eqs.(26) and (27).

**Fig.14:** (a) typical transversal tensile failure of the analyzed laminae under transversal compressive loading; (b) transversal compressive strength and theoretical models given by Eqs.(31) and (32).

**TABLE CAPTIONS**

**Tab.1:** Elastic properties of the sisal fiber.

**Tab.2:** Mechanical strength of the sisal fiber.

**Tab.3:** Micromechanical models to predict the elastic properties of the unidirectional lamina

**Tab.4:** Micromechanical models to predict the mechanical strength of the unidirectional lamina.

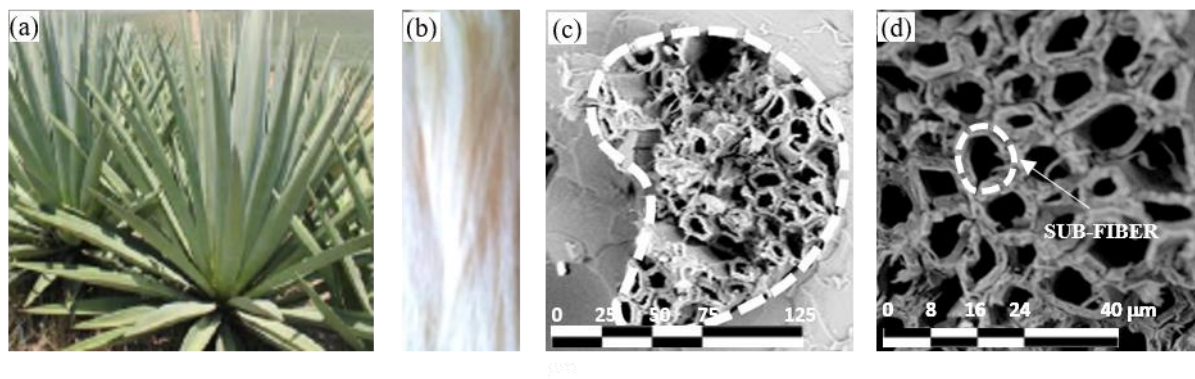


**Fig.1.** (a) plants of agave sisalana, (b) fibers, (c) typical horseshoe fiber section and (d) hollow cylindrical sub-fibers.



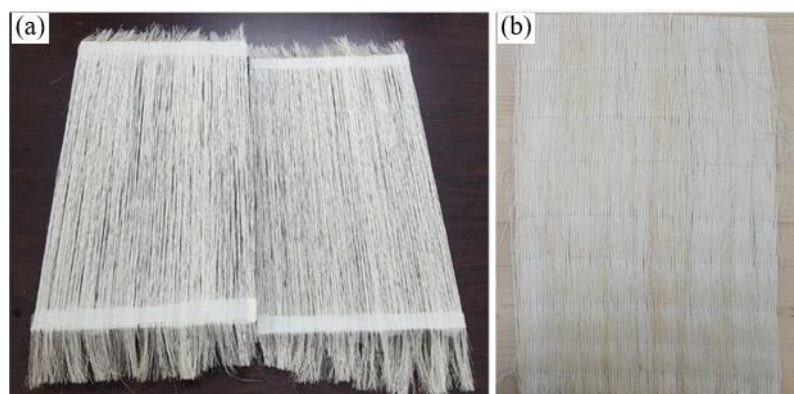


**Fig.2.** Unidirectional stitched fabric made on laboratory: (a) alignment and stretching of the fibers, (b) fabric after transversal stitching.

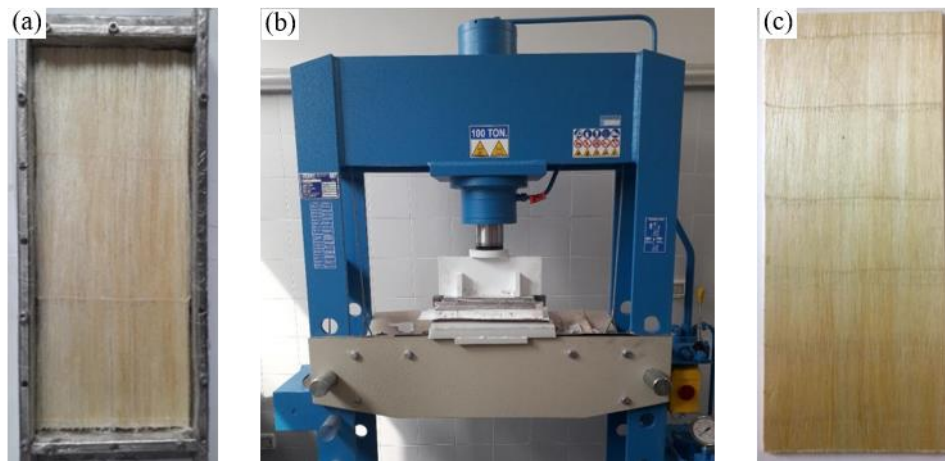


**Fig.3.** Biocomposite manufacturing: (a) hand lay-up inside the mold, (b) mold, counter-mold and press used for the thermo-mechanical compression moulding and (c) biocomposite panel obtained.

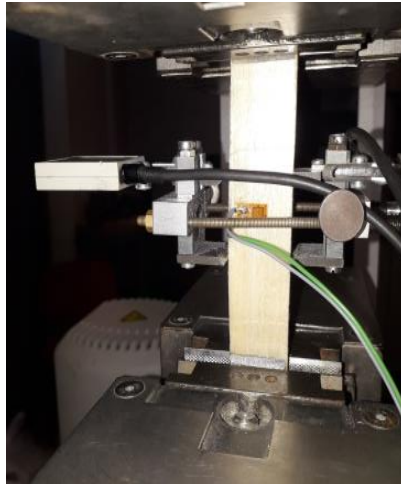


**Fig.4.** Longitudinal and transverse tensile tests performed by using an INSTRON 3367 material test machine and specimens instrumented by a micrometer type HBM and a transversal ER type VISHAY.

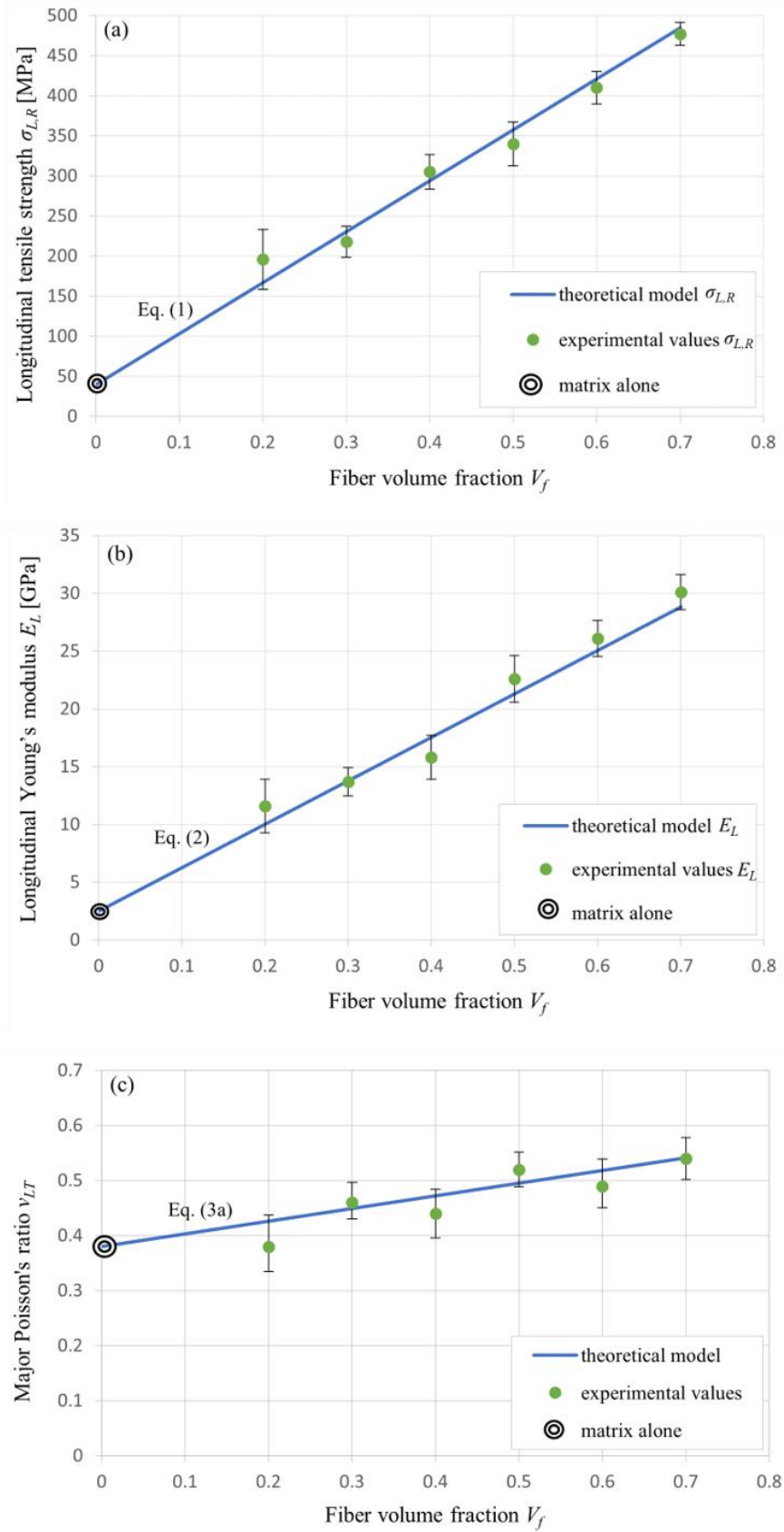


**Fig. 5.** (a) Longitudinal tensile strength and theoretical ROM models represented by Eq. (1); (b) longitudinal Young's modulus and theoretical model represented by Eq. (2); (c) major Poisson's ratio and theoretical model given by Eq. (3a).

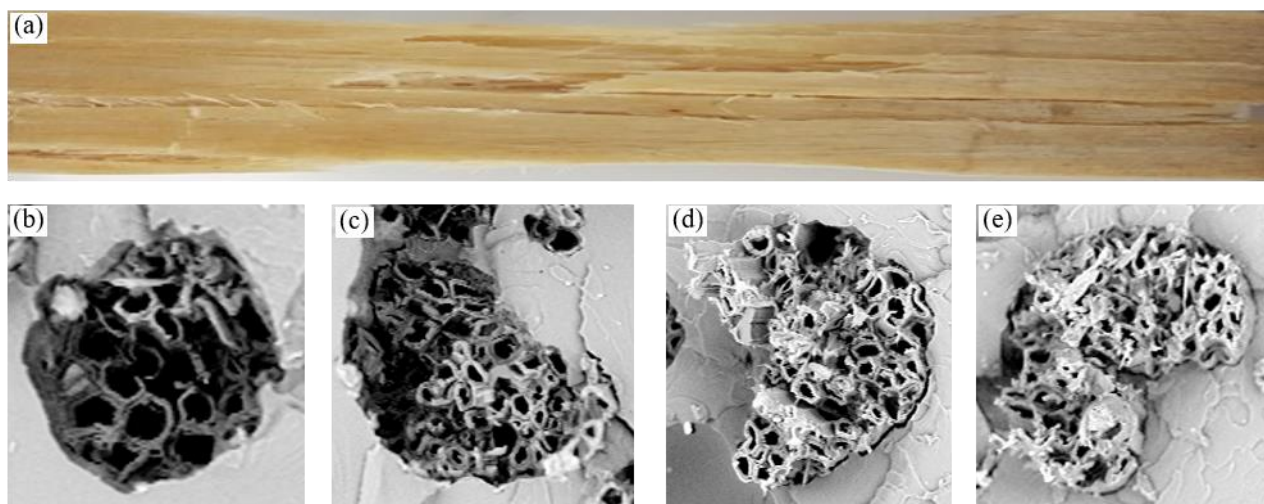


**Fig.6.** (a) Typical image of specimens fractured by tensile test and (b-e) SEM micrographs of the corresponding fracture surfaces.

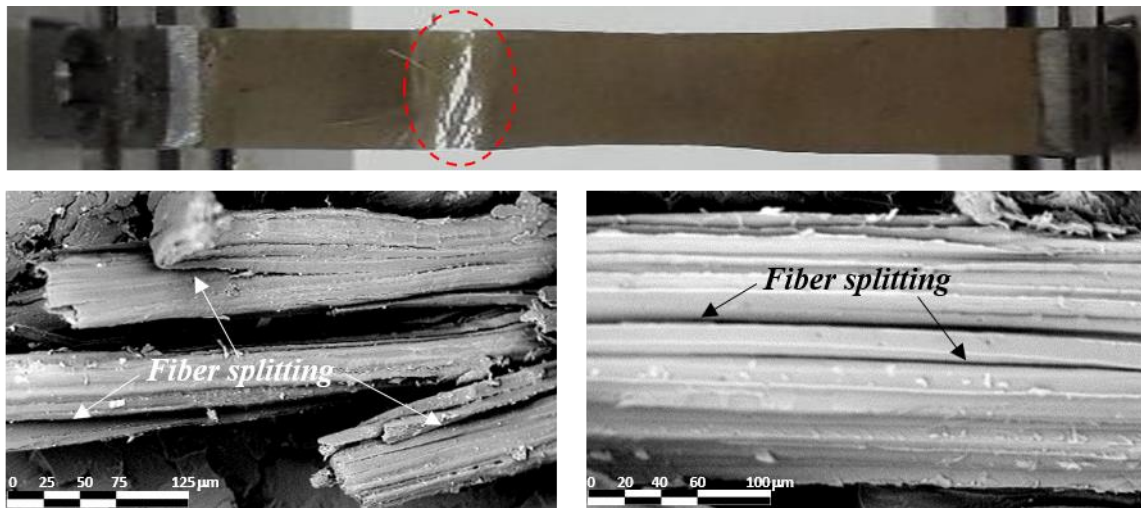


**Fig.7.** (a) Typical image the specimens after transversal tensile test and  
(b, c) SEM micrographs of the fracture surfaces that evidence the fiber splitting.

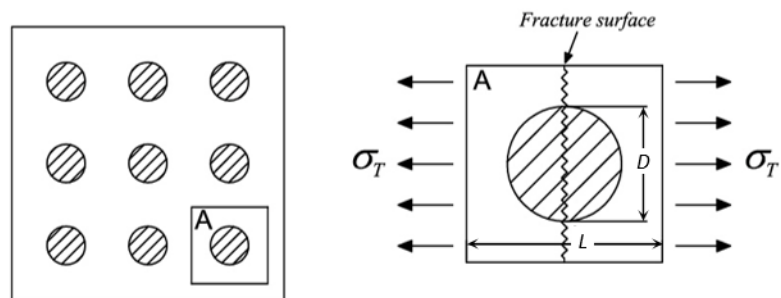


**Fig.8.** PMM: (a) typical model scheme and (b) RVE used for the analysis of the transversal tensile strength.

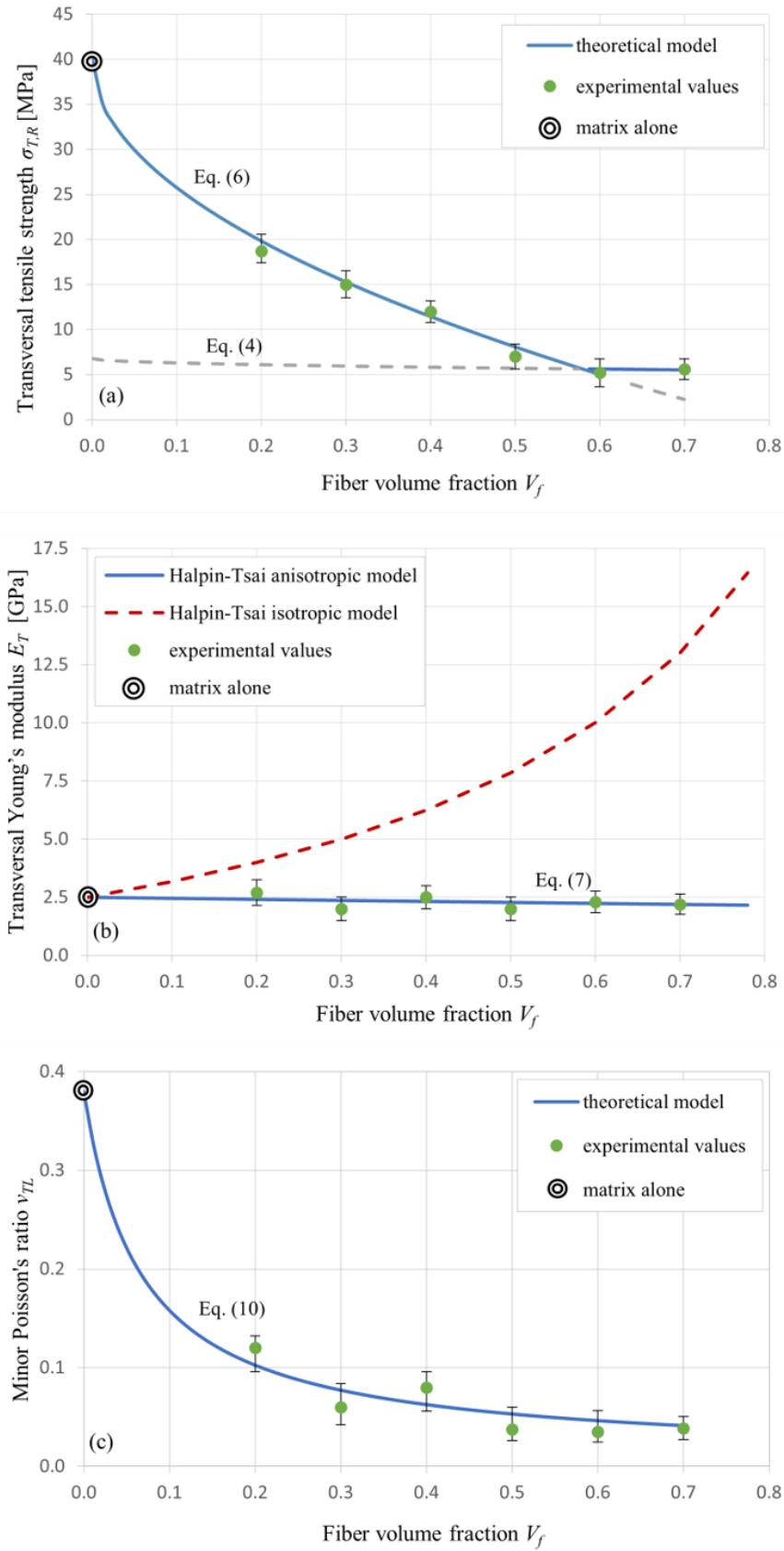


**Fig.9.** (a) Transversal tensile strength and theoretical models obtained by PMM; (b) transverse Young's modulus and Halpin-Tsai models; (c) minor Poisson ratio  $\nu_{TL}$  and model provided by micromechanics.



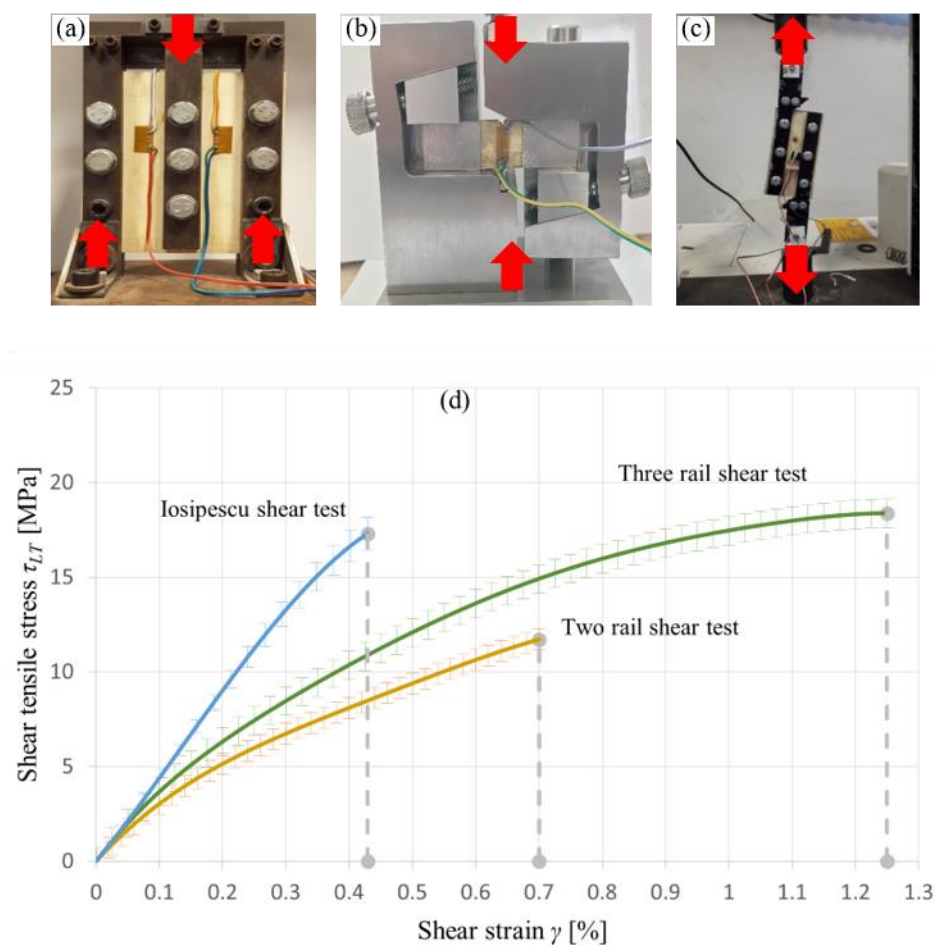


**Fig.10:** Shear tests: (a) three rail shear test, (b) Iosipescu shear test, (c) two rail shear test and (d) mean shear curves relative to the unidirectional lamina biocomposite with  $V_f = 70\%$ .

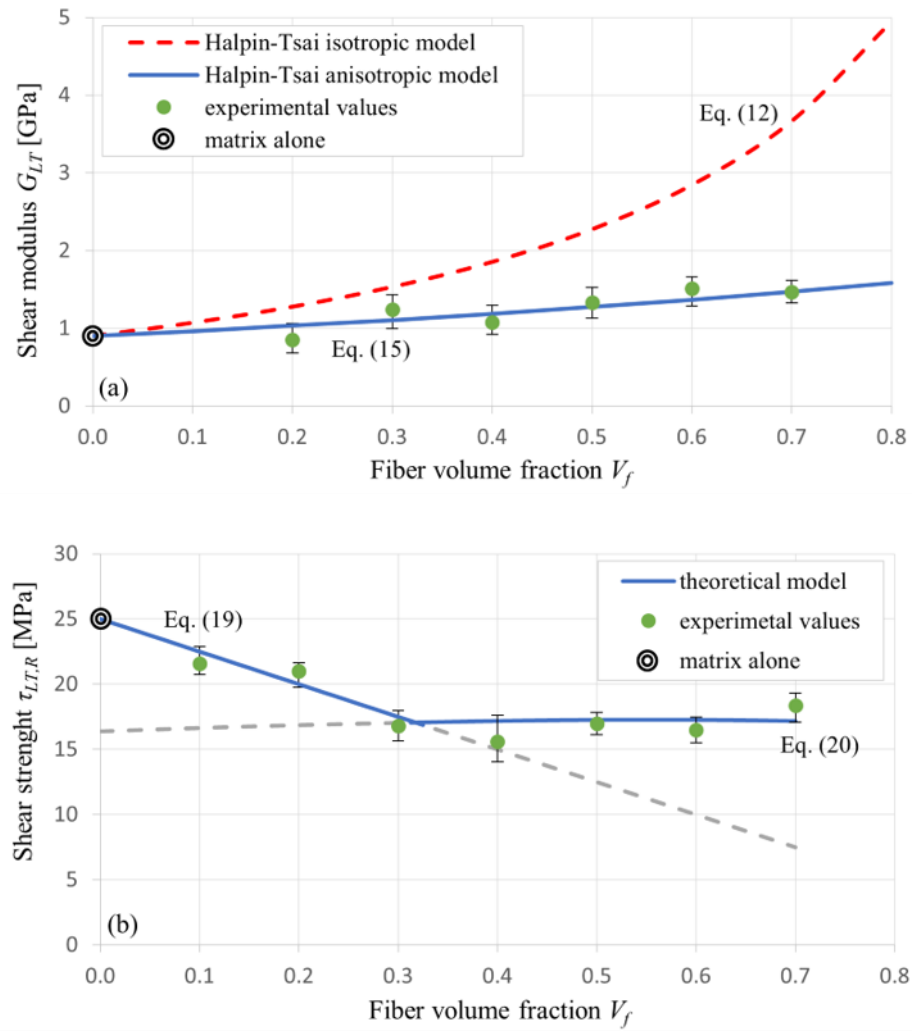


**Fig.11:** (a) Shear modulus of the analyzed biocomposite laminae versus  $V_f$ , and Halpin-Tsai models; (b) shear strength versus  $V_f$  and theoretical models proposed.

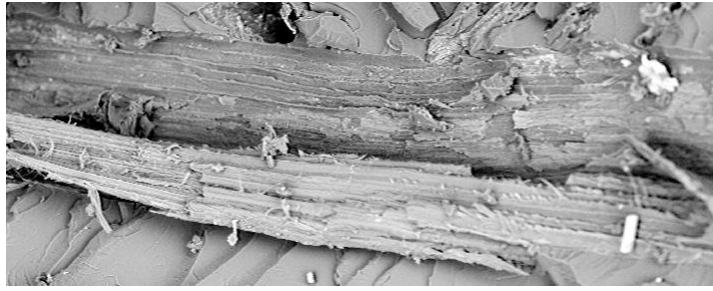


**Fig.12:** SEM micrographs of the fracture surface of the analyzed specimens under shear loading, showing the typical internal fiber splitting.

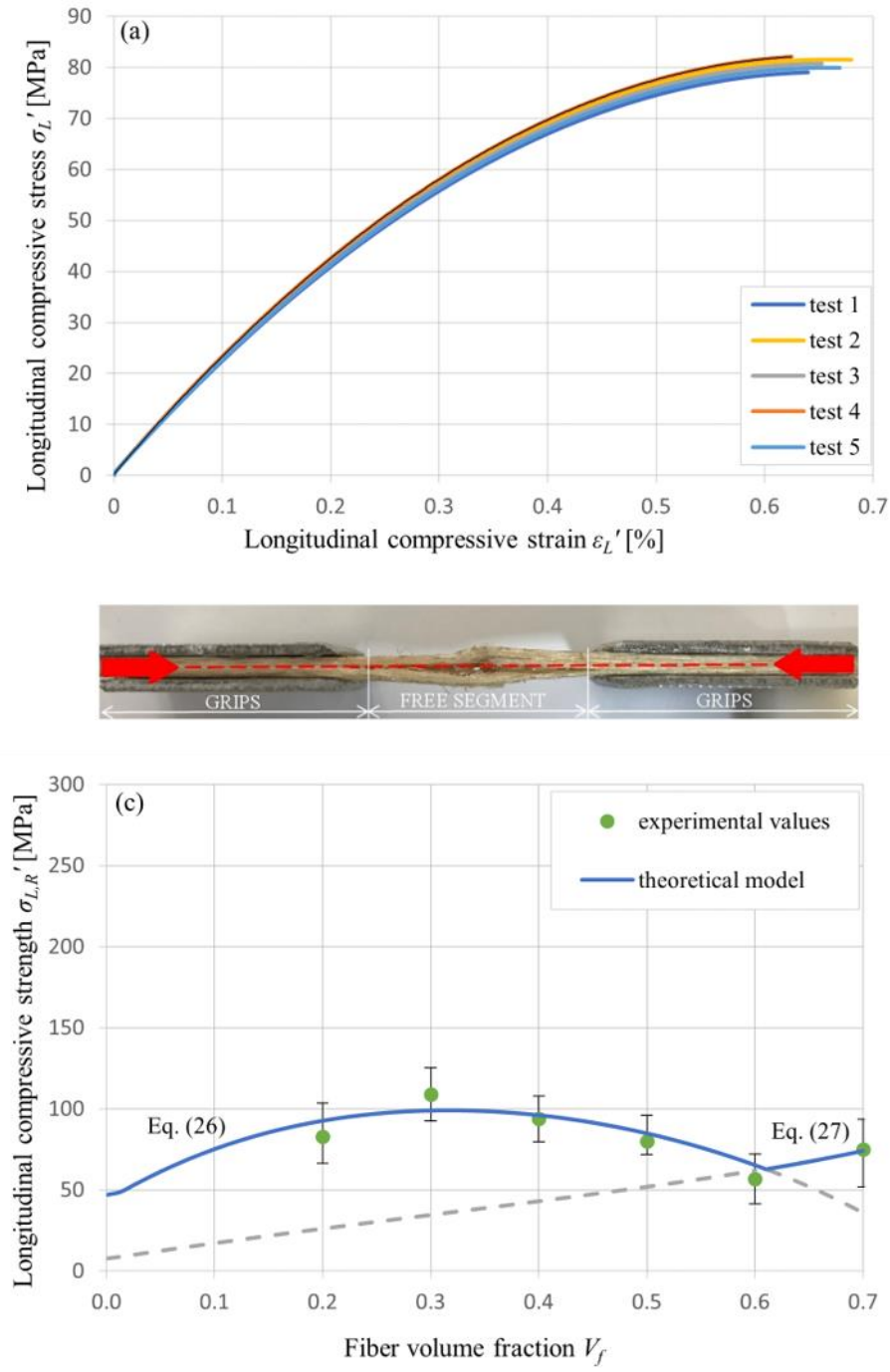


**Fig.13:** (a) typical longitudinal compressive curves for the biocomposite examined ( $V_f = 0.5$ ); (b) typical transversal tensile failure; (c) longitudinal compressive strength vs.  $V_f$  and theoretical models given by Eqs. (26) and (27).

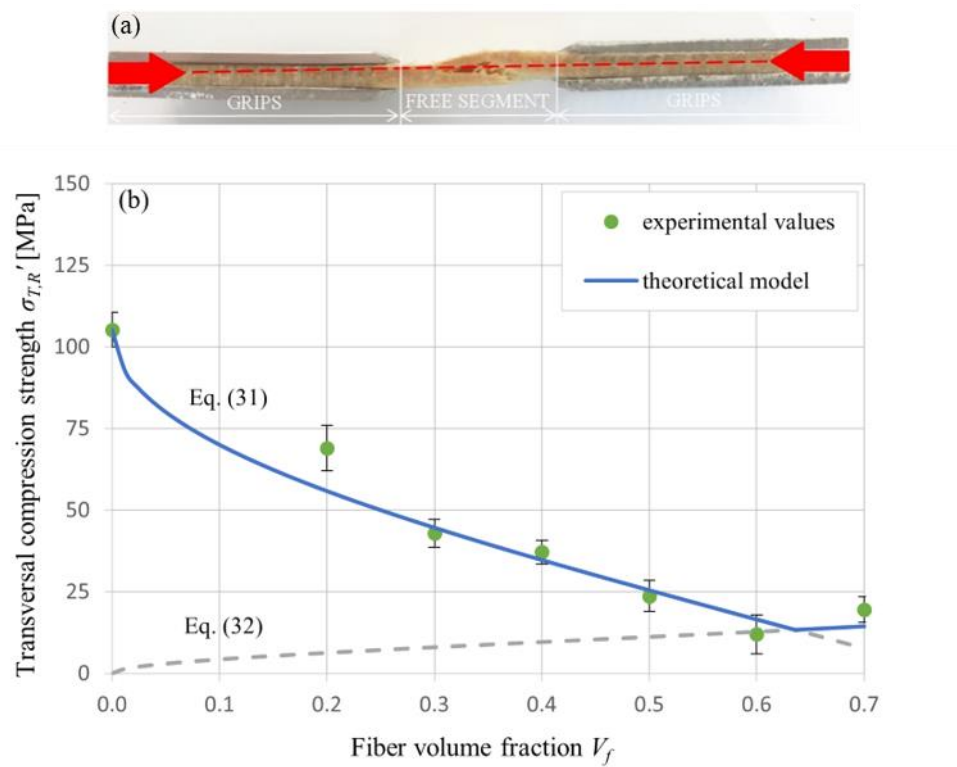


**Fig.14:** (a) typical transversal tensile failure of the analyzed laminae under transversal compressive loading; (b) transversal compressive strength and theoretical models given by Eqs.(31) and (32).

**Tab.1:** Elastic properties of the sisal fiber.

$E_L^{(f)}$ [GPa]	$E_T^{(f)}$ [GPa]	$G_{LT}^{(f)}$ [GPa]	$\nu_{LT}^{(f)}$	$\nu_{TT}^{(f)}$	$E_L'^{(f)}$ [GPa]	$E_T'^{(f)}$ [GPa]
40.1	2.07	1.84	0.61	0.21	40.1	2.07

**Tab.2:** Mechanical strength of the sisal fiber.

$\sigma_{L,R}^{(f)}$ [MPa]	$\sigma_{T,R}^{(f)}$ [MPa]	$\tau_{LT,R}^{(f)}$ [MPa]	$\sigma_{L,R}'^{(f)}$ [MPa]	$\sigma_{T,R}'^{(f)}$ [MPa]
675	5.55	19.1	-	-

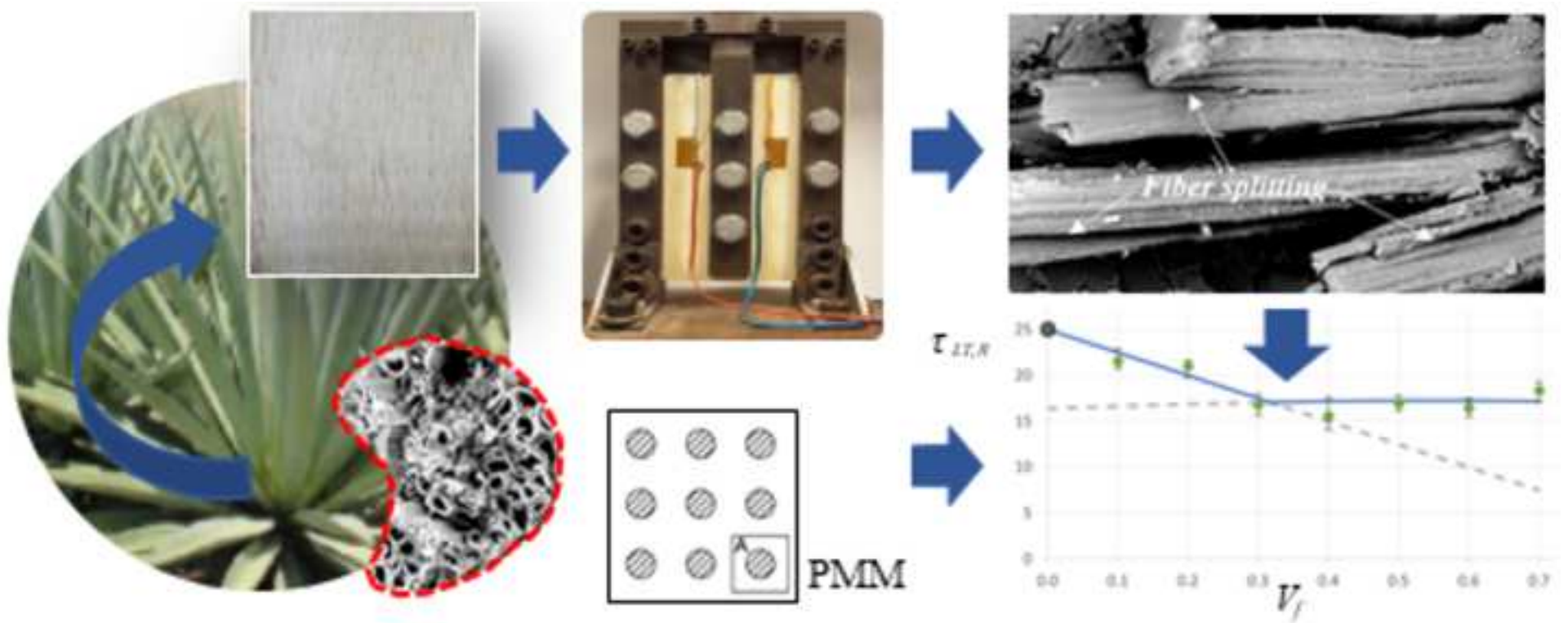
**Tab.3:** Micromechanical models to predict the elastic properties of the unidirectional lamina.

$E_L$	$E_T = E'_T$	$\nu_{LT}$	$G_{LT}$	$\nu_{TT}$	$E'_L$
Rule of mixture (Eq.2)	Anisotropic Halpin-Tsai rule (Eq.7)	Rule of mixture (Eq.3a)	Anisotropic Halpin-Tsai rule (Eq.14)	Compliance averaging model (Eq.29)	Micromechanical formula (Eq.23)



**Tab.4:** Micromechanical models to predict the mechanical strength of the unidirectional lamina.

$\sigma_{L,R}$	$\sigma_{T,R}$	$\tau_{LT,R}$	$\sigma'_{L,R}$	$\sigma'_{T,R}$
Corrected rule of mixture (Eq.1)	Periodic microstruct. model (Eqs.4 and 6)	Periodic microstruct. model (Eqs.18 and 19)	Transversal tensile failure model (Eq.25 and 26)	Transversal tensile failure model (Eq.30 and 31)



## **Highlights**

- 1) Anisotropy of the sisal, also in term of mechanical strength, has been highlighted
- 2) Observed splitting phenomena affects the main mechanical properties of the lamina
- 3) SEM analyses corroborate that splitting affects also shear and compressive strength
- 4) The experimental results have allowed to implement reliable micromechanical models
- 5) The main mechanical parameters useful at the biocomposite design stage, are given

### **CRedit authorship contribution statement**

**Bernardo Zuccarello:** Term, Conceptualization, Methodology, Validation, Supervision, Project administration, Writing - Review & Editing. **Carmelo Militello:** Investigation, Data Curation, Validation, Writing - Review & Editing. **Francesco Bongiorno:** Investigation, Data Curation, Validation, Visualization, Writing - Original Draft.